Metallic Interconnects for Proton Ceramic Fuel Cells

Oxidation behavior and transport properties under simulated fuel cell conditions

Anders Werner Bredvei Skilbred

Dissertation for the degree of Philosophiae Doctor

Centre for Materials Science and Nanotechnology
(SMN)

Department of Chemistry
Faculty of Mathematics and Natural Sciences

UNIVERSITY OF OSLO

2012

Series of dissertations submitted to the
Faculty of Mathematics and Natural Sciences, University of Oslo
No. 1279

ISSN 1501-7710

Cover: Inger Sandved Anfinsen.
Printed in Norway: AIT Oslo AS.

Produced in co-operation with Akademika publishing.
The thesis is produced by Akademika publishing merely in connection with the thesis defence. Kindly direct all inquiries regarding the thesis to the copyright holder or the unit which grants the doctorate.

Preface

This thesis represents parts of the requirements for the degree of Philosophiae Doctor (Ph. D.) at the Department of Chemistry, Faculty of Mathematics and Natural Sciences, University of Oslo. This work has been funded by the Research Council of Norway, and has been carried out at Functional Energy Related Materials in Oslo (FERMiO) at the Centre for Materials Science and Nanotechnology (SMN).

I would like to thank my two supervisors: Reidar Haugsrud for countless hours of consultancy services at any time of day. You have accomplished to make a handy-man from Stokke into a published scientist. I'm impressed with your unstoppable enthusiasm, drive and care both when it comes to science, life and skiing. I'm also grateful to Truls Norby who has guided me with enthusiasm and interest since my first semester at UiO. Yngve Larring and Sen Mei at SINTEF also deserve my gratitude for support and cooperation in the StackPRO project.

I would also like to express my gratitude to Prof. David J. Young and Dr. Jianqiang Zhang who I was so fortunate to work with at the University of New South Wales, Sydney, for three months in the autumn of 2009. My fellow PhD students Philip Speck and Thomas Gheno is acknowledged for making my stay valuable both with regards to science and social activities.

Further, I want to thank all my brilliant colleagues and the students in the group of Solid State Electrochemistry. You are all exceptional! A special thanks' to Tor Svendsen Bjørheim, Vasileios Besikiotis and Harald Fjeld for numerous discussions with and especially without scientific content.

I'm truly grateful to my parents and the rest of my continuously growing family. Thank you for all your support and care. I also wish to acknowledge my late grandfather, Ole Jacob, for his important influence on my choices through life.

Further, I would like to thank Sigrid for her highly efficient distractions and unconditional love. And finally, I will thank Kristin Elise for her love, support and patience. Together we are strong and clever. I love you!

Oslo, September 2012

Anders Werner Bredvei Skilbred

Summary

Fuel cells are expected to serve as a contribution to meet the demand for clean energy. High temperature fuel cells such as solid oxide fuel cells (SOFC) and proton ceramic fuel cells (PCFC) are developed for use as environment friendly energy conversion devices. However, the successful implementation of such devices in practical applications relies on series connections of multiple cells by so-called interconnects. During operation at high temperatures (600 – 850 °C) facing both air and fuel, oxidation of these metallic interconnect materials is inevitable. Formation of oxide scales will result in a reduced overall performance of the fuel cell stack. It is therefore crucial to investigate the oxidation behavior and the mechanisms responsible for the oxide growth on the interconnect.

This thesis consists of six chapters where the first five chapters give the basis for the work presented in five articles. Chapter six presents a summarizing discussion which links the results from PAPER I – IV and discusses them further, and to some extent in more speculative terms than found suitable in the individual papers.

The applicability of a material as an interconnect for SOFC and PCFC rely on several high temperature materials' properties. Some of the most essential properties were investigated in this study for the Sandvik Sanergy HT. It was found that the thermal expansion was ~12.5×10^{-6} /°C, a value that is regarded as suitable for SOFC and PCFC application. Further, it was found that due to the limited formation of electrical resistive oxide scales, the area specific resistance (ASR) measured at 700 °C was as low as ~6 mOhm×cm^2 after 500 h in wet air. This is below the generally regarded threshold value of 10 mOhm×cm^2 for interconnect materials.

The oxidation behavior of Sanergy HT was thoroughly investigated throughout this thesis. Up to 900 °C the oxidation behavior showed parabolic kinetics, whereas at 1000 °C the oxidation process was accelerated after ~300 h. The activation energy for oxidation (800 – 900 °C) was found to be 272±20 kJ/mol. The oxide scales formed during oxidation in air comprised an inner layer of Cr_2O_3 and an outer layer of $(Cr,Mn)_3O_4$-spinel.

Two-stage oxidation experiments were performed where the first stage of oxidation was in $^{18,18}O_2$ (g) and the second stage was in $^{16,16}O_2$ (g) in order to elucidate the oxide growth mechanisms. SIMS profiles revealed that the governing transport mechanism responsible for oxide growth was outward cation diffusion. Oxygen tracer diffusion experiments showed that inward diffusion of oxygen was significant in the outer region of the oxide scale. As a result of outward cation transport through the inner layer of Cr_2O_3 and inward oxygen diffusion through the outer layer comprising $(Cr,Mn)_3O_4$ it was suggested that the oxide growth takes place within the scale, likely near the Cr_2O_3 - $(Cr,Mn)_3O_4$ interface. However, the diffusion of cations through the inner chromia layer is still regarded as the rate limiting mechanism for the oxidation process.

During operation in a fuel cell the interconnect is facing air on the cathode side and fuel on the anode side simultaneously. Such dual atmosphere exposures have been found to significantly alter the oxidation behavior of the interconnect on the cathode side as a result of transport of hydrogen species through the alloy. This was identified by an extensive formation of Fe-rich oxide nodules, accompanied by localized internal oxidation and metal loss. The influence of dual atmosphere was further enhanced by increasing the water vapor content in the air on the cathode side. Introducing water vapor on the anode side gave however the opposite effect; less extensive nodule formation and metal attack. Further, it was observed that the preferred location of nodule formation and internal oxidation was related to surface

deformations of the as received samples left by cold work during fabrication, *e.g.* the rolling process. Interestingly, dual atmosphere conditions was not found to have any significant effect on the oxidation of samples coated with a metallic layer of Ce (10 nm) with Co (800 nm) on top.

The anomalous oxidation behavior of uncoated samples encountered under dual atmosphere conditions was suggested to be a breakaway type of oxidation. The transport of hydrogen through the alloy increases the H_2O (g)/O_2 (g) ratio near the metal – oxide interface and triggers breakaway oxidation, identified by internal oxidation, metal attack and formation of Fe-rich oxide phases observed as nodules. The reduced effect of dual atmosphere conditions on coated samples was suggested to be due to a combination of reduced hydrogen transport through the coated samples, and a decreased susceptibility towards breakaway oxidation as a result of a reduction in the chromium evaporation.

Chromium nitrides are known to improve mechanical and chemical properties of alloys. It has therefore been suggested that the formation of CrN_x on interconnects could also improve the high temperature performance of these materials. The literature on thermal nitridation of chromium bearing alloys is limited, and in order to contribute to a more fundamental understanding of this subject ten Fe-Cr, Ni-Cr and Fe-Ni-Cr model alloys and two ferritic interconnect materials were treated at high temperatures in an atmosphere containing a mixture of nitrogen and hydrogen. It was found that the extent of internal precipitation of Cr_2N increased with increasing chromium content, except for the ternary Fe-Ni-Cr alloys. It was also found that the nitridation kinetics were generally slower for the nickel bearing alloys. Chromium nitrides were formed on the surface of the ferritic interconnects proving that thermal nitridation is a possible technique to form an external Cr_2N layer on commercial

interconnect alloys. The potential effect on the high temperature properties of these materials was not further investigated.

On the basis of the investigations presented in this thesis the Sandvik Sanergy HT may be a good candidate interconnect material for PCFC. The TEC of the alloy is regarded suitable for PCFC, however this depends on the other materials used in the fuel cell assembly. At lower temperatures (700 - 800 °C) the alloy proves good oxidation resistance and the oxide scales formed holds rather good electrical conductivity (~6 $m\Omega cm^2$ after 500 h at 700 °C). The predicted lifetime of the interconnect far exceeds the expected lifetime of the fuel cell (>50 000 h). At higher temperatures (>800 °C) the effect of dual atmosphere exposures is significant, and is likely to accelerate the degradation of the performance of the interconnect if used in SOFC. However, the temperature regime of PCFC (600 – 700 °C) is regarded to result in slow oxide growth kinetics, and dual atmosphere environments may therefore not significantly affect the performance of the material. Any effects of dual atmosphere conditions is likely to be reduced by application of metallic Ce/Co coatings, also improving the overall performance of the fuel cell stack.

The application of metallic Ce and Co coatings is regarded as a beneficial and likely improvement of performance of the Sanergy HT, both with respect to limited chromium evaporation and reduced the effects of dual atmosphere.

Contents

1 Introduction

Motivation

During the last decades a growing concern for increasing global temperatures has been raised by the climate research community worldwide. There is a broad scientific consensus that the rising temperatures are consequences of increased concentrations of greenhouse gases in the atmosphere, especially carbon dioxide, CO_2. CO_2 is released by the combustion of fossil fuels, and the emission increase has followed the development of the modern society starting with the industrial revolution. The energy consumption of the world is still increasing, and is predicted to continue to do so on an average of ~2 % per year from 2003 to 2030 [1]. The most rapid growth in energy demand is projected to be found in nations outside the OECD, often recognized by fast growing economy and old energy technology. It is therefore of critical interest to develop new energy conversion systems based on renewable energy sources that are affordable and competitive, and can ensure a sustainable global development.

Fuel cells

In order to meet the increasing energy demand by utilizing cleaner energy resources, a wide range of renewable energy technologies are called for. Fuel cells can offer a clean and environment friendly conversion of energy.

Much like an ordinary battery, a fuel cell is a galvanic cell that converts chemical energy stored in a fuel into electricity (and heat) without combustion. It is built up of four basic

components; electrolyte, two electrodes (anode and cathode) and interconnect. However, unlike a battery which is in principle a closed system, a fuel cell is an open system that is continuously fed with fuel. This enables continuous production of electricity as long as fuel is provided.

The most widely commercial available type of fuel cells is the polymer exchange membrane fuel cell (PEM-FC). This low temperature fuel cell (typically < 120 °C) is based on aqueous transport of hydrogen through a membrane electrolyte, with a proton conductivity in the range of 0.1 S/cm [3]. However, due to the low operation temperature and the working principle of the membrane, the PEM-FC is vulnerable towards contamination and impurities in both the fuel and oxidant gases. Hence, only pure and clean hydrogen and oxygen (and to some extent air) can be utilized. High temperature fuel cell systems are generally more robust towards challenges regarding impurities and contamination. Furthermore, by increasing the operation temperature to above 500 °C fuel flexibility and utilization can be improved *e.g.* by enabling use of hydrocarbons as alternative fuels.

High temperature solid oxide fuel cells, SOFCs, have been under extensive investigations for several decades. Traditionally, an SOFC is a term describing a high temperature fuel cell based on an oxide ion conducting electrolyte. During operation, oxide ions are transported through the electrolyte from the cathode side (air) to the anode side (fuel) forming water in the fuel by the reaction between oxide ions and hydrogen on the anode. This results in a dilution of the fuel, reducing the fuel utilization. The most widely used SOFC is based on an yttria stabilized zirconia electrolyte (YSZ). State-of-art YSZ SOFC has a target oxygen ion conductivity of 0.1 S/cm at 750 °C. However, the high operating temperatures are regarded as a general disadvantage of the YSZ SOFC, although a substantial research effort has resulted

in decreasing the typical operation temperature from ~1000 °C to ~750 °C making the SOFC a more realistic alternative for green energy conversion.

In a proton ceramic fuel cell (PCFC) the oxide ion conducting electrolyte is replaced with a proton conducting material. Protons are transported from the fuel on the anode side to the air on the cathode side, forming water in the reaction between protons and oxygen. The main benefit of the PCFC compared to the more traditional SOFC is that the dilution of fuel is avoided, thus significantly increasing the fuel efficiency. Another advantage of the PCFC over the conventional SOFC is a potentially lower operation temperature, which facilitates the use of less complex and costly materials in the fuel cell assembly. However, there are still challenges to overcome regarding the performance of the PCFC. State-of-art PCFC electrolyte candidate material, Y-doped $BaZrO_3$, is reported to have a proton conductivity of $\sim 1\times10^{-2}$ S/cm at 450 °C [4]. However, high grain boundary resistance and Ba evaporation at high temperatures (*e.g.* during fabrication) are major concerns for this type of materials.

Norway has for the last 10 years been an important contributor to the development of PCFC, with focus on proton conducting oxides as efficient electrolytes. Numerous materials have been in the searchlight, but only a few have been considered promising. One of these materials is $LaNbO_4$ which combines rather high proton conductivity ($\sim 1\times10^{-3}$ S/cm at 900 °C for $La_{0.99}Ca_{0.01}NbO_4$) with a superior chemical stability compared to its Ba containing proton conducting competitors [5]. Based on the promising properties of $LaNbO_4$ a number of projects have been started within the so called “PCFC package” with the scope of identifying, characterizing and develop materials for a novel and efficient PCFC assembly.

Interconnects

In practical applications individual fuel cells are stacked in series in order to provide usable power, where so called interconnects separate the individual cells. The main purpose of the interconnect is to provide electrical contact between the anode and cathode, as well as to separate the fuel from the air. This requires a gas tight material with high electronic conductivity and mechanical strength, even after long term high temperature operation facing both oxidizing and reducing atmospheres.

Metallic interconnects, based on stainless steels, are proposed to be used in fuel cells with working temperatures below 800 °C. During operation at elevated temperatures formation of oxide scales is inevitable, and these layers have different properties with regards to the electrical conductivity, thermal expansion and mechanical strength as compared to the initial metallic interconnect material. Consequently, the formation of these oxide scales can significantly deteriorate the performance of the fuel cell stack. It is therefore of great importance to attain detailed knowledge about the oxidation processes and the properties of the formed oxide scales.

This thesis is based on five manuscripts that describe various high temperature properties and aspects of the oxidation and corrosion of bare and coated ferritic stainless steels used as interconnects in solid oxide fuel cells and some other selected un-coated alloys. This represents some of the work done in the StackPro project that was started with the aim of identifying and characterizing candidate interconnect materials, and to develop a functional PCFC stack as a proof-of-concept consisting of at least two interconnected fuel cells.

2 Oxidation of metals and alloys

The field of high temperature oxidation and corrosion of metals and alloys is vast, and the following chapter will only briefly discuss some of the most essential contributions to our understanding of this topic and the literature most relevant to this thesis. For a more comprehensive overview of this fascinating field of science additional sources of literature are recommended [6-9].

Oxidation of metals

Oxidation of metals by reaction with oxygen is in principle one of the simplest chemical reactions and can for a general metal, M, be written:

$$aM + \frac{b}{2} O_2 \rightarrow M_a O_b \qquad \text{Eq. 1}$$

The oxidation reaction is initiated by adsorption of oxygen on the metallic surface, followed by an initial transient stage where all components in an alloy will oxidize. During the initial nucleation and growth, a thin oxide layer forms and covers the entire metal surface. Surface defects and impurities in the metal and/or the gas will influence the adsorption of oxygen, nucleation and formation of the oxide. When a continuous and dense oxide scale is formed, further oxidation of the metal can only proceed by solid state diffusion of oxygen and/or metal through the oxide scale barrier. The relative rate of anion and cation transport through the oxide scale, and thus the predominating defect situation in the oxide, will dictate whether growth of the oxide scale mainly occurs at the metal – oxide interface (dominated by inward

oxygen transport) or at the oxide – gas interface (outward cation diffusion), or a mixture of the two. For very thin oxide scales, the driving force for diffusion is electric fields, while growth of thicker scales is driven by chemical potential gradients.

2.1.1 Thermodynamics

The stability of an oxide, and thereby whether it will form or not, can be determined by considering the *Gibbs free energy*, G , of the system. The change in Gibbs free energy for a reaction (*e.g.* oxidation of metal) can be written (when temperature and pressure is constant):

$$\Delta G = \Delta H \text{ - } T\Delta S \qquad \text{Eq. 2}$$

where ΔH and ΔS are the change in enthalpy and entropy, respectively, for the reaction. The standard free energy, ΔG^0, for the formation of oxide per mole of oxygen is expressed as:

$$\Delta G^0 = -RT\ln\left(\frac{a_{M_aO_b}}{a_M^a a_{O_2}^{b/2}}\right) \qquad \text{Eq. 3}$$

The activities of the solids, $a_{M_aO_b}$ and a_M are defined equal to unity, while the activity for a gas, in this case oxygen, a_{O_2}, is given by its partial pressure, p_{O_2}, leading to the equation:

$$\Delta G^0 = -\frac{b}{2} RT \ln p_{O_2} \qquad \text{Eq. 4}$$

Due to the negative standard entropies for the formation of metal oxides, a plot presenting ΔG^0 as a function of temperature gives a straight line with a positive slope, indicating that

the stability of the oxides decreases with increasing temperature. The most stable oxides in such a diagram will be characterized by the most negative ΔG^0 values.

From a thermodynamics point of view an oxide will only form when the oxygen partial pressure is similar to or larger than the dissociation pressure of the oxide, *i.e.* when the metal and oxide coexist:

$$p_{O_2} \geq \exp\left(\frac{\Delta G^0}{b\mathrm{R}T}\right) \qquad \text{Eq. 5}$$

A useful presentation of standard free energies for the formation of selected oxides is an *Ellingham-Richardson diagram* as shown in Fig. 1 [10]. By using this diagram stabilities of oxides can be compared and the values of dissociation pressures can be obtained directly. This information can be used to identify which element of an alloy that will form the most stable oxide and is thereby likely to act as a protective corrosion resistant oxide layer on the base alloy.

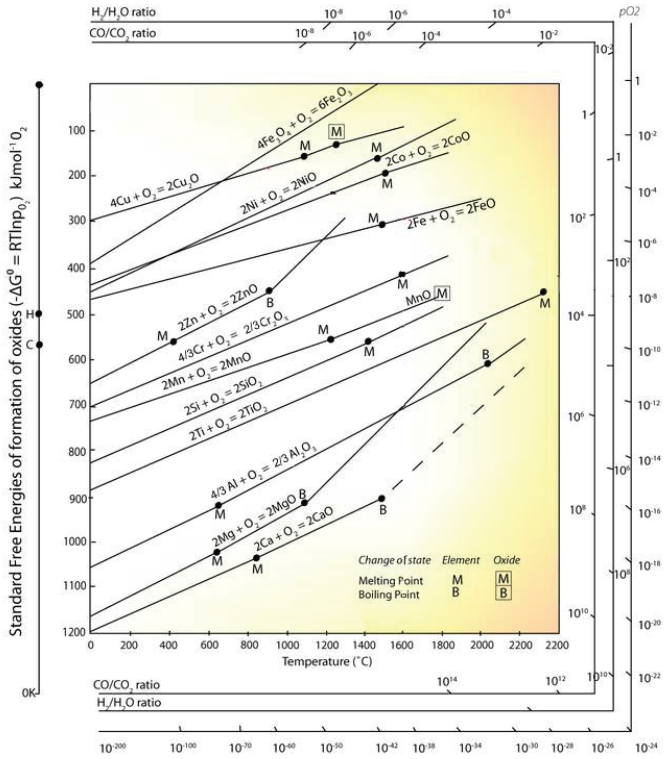

Fig. 1. Ellingham-Richardson diagram showing free energies for formation of selected oxides as a function of temperature.

2.1.2 Oxidation kinetics

Although the thermodynamic stability of an oxide dictates whether or not it will form, the rate of oxidation and scale growth is given by the kinetics of the oxidation process. Oxidation of metals and alloys is often found to follow a parabolic time dependence, which empirically may be described by[11]:

$$\frac{dx}{dt} = k'_{p,t} \frac{1}{x} \qquad \text{Eq. 6}$$

Integration over time yields:

$$x^2 = 2k'_{p,t} + C_0 = k_{p,t} + C_0 \qquad \text{Eq. 7}$$

where x is the oxide scale thickness, $k_{p,t}$ denotes the parabolic rate constant and C_0 is an integration constant. The parabolic law (Eq. 6) describes an oxidation process governed by the lattice diffusion of the reactant through the oxide scale. Due to the continuously increasing thickness with time, the diffusion paths of the migrating species increases, and the reaction rate decreases.

Oxidation rates typically show Arrhenius-type temperature dependencies at constant oxygen partial pressures, and can be expressed by:

$$k = k_0 e^{\frac{-E_a}{RT}} \qquad \text{Eq. 8}$$

Rate constants determined at various temperatures thus enables determination of the activation energy for oxide growth, E_a, by plotting values for parabolic rate constants as a function of inverse temperature [7]. A constant activation energy may imply that the same oxidation mechanism predominates the oxidation process throughout the experimental temperature interval. An overall temperature dependence deviating from the Arrhenius behavior may similarly indicate a changeover between two limiting processes within a certain temperature interval, for instance from inward oxygen diffusion to outward transport of cations [12].

Wagner theory

The first fundamental theory for describing oxidation kinetics was developed by Carl Wagner, and published ten years after the empirically described parabolic law [13]. Wagner based his theory on the assumption that lattice diffusion of electrically charged species is rate limiting for the oxidation process [8]. Accordingly, the oxide formed must be dense, continuous and perfectly adherent. Although the scale shows only small deviations from stoichiometry defects in the oxide allow for migration. At both the metal – oxide and oxide – gas interface reactions are assumed to be rapid, and local equilibria are established. Both ions and electrical species are assumed to migrate independently, and the net electrical current is defined as zero. Wagner's original equation for metal oxidation is written:

$$k_p = \int_{a_O^{/}}^{a_O^{//}} D_M \frac{Z_M}{|Z_O|} \mathrm{d} \ln a_O \qquad \text{Eq. 9}$$

where D_M is the self-diffusion coefficient of the metal, $a_O^{/}$ and $a_O^{//}$ represents the oxygen activities at the metal – oxide and oxide – gas interface, respectively. This expression that can be modified to describe a number of oxidation situations, *e.g.* the oxidation of a metal deficient oxide, $M_a O_{b-\delta}$, dominated by metal vacancies can be written:

$$k_{p,t}^{/} \approx \frac{D_{v_M}}{b} \int_{\mathrm{p}O_2^{/}}^{\mathrm{p}O_2^{//}} \delta d \ln p_{\mathrm{O}_2} \qquad \text{Eq. 10}$$

where $k_{p,t}^{/}$ denotes the thickness related parabolic rate constant. In many studies of oxidation kinetics weight gain due to oxygen uptake of a sample is measured, giving the weight related parabolic constant, $k_{p,w}^{/}$. These two parabolic growth rates are related via the molecular mass of oxygen, M_O, the oxide, $M_{M_aO_b}$, and its density, $d_{M_aO_b}$:

$$k'_{p,w} = \left(\frac{M_{M_aO_b}}{b \cdot M_O \cdot d_{M_aO_b}} \right)^2 \cdot k'_{p,t} \qquad \text{Eq. 11}$$

As previously described, Wagner's oxidation theory is based on several assumptions and is only valid when oxidation occurs under ideal conditions. However, the model has proven to be remarkably accurate and versatile for describing oxide scale growth kinetics of numerous metals and alloys under real conditions.

2.1.3 Diffusion

Diffusion is described by Fick's laws, where the first law is written:

$$J = -D \frac{\partial C}{\partial x} \qquad \text{Eq. 12}$$

It relates the flux of the diffusing species, J, with the diffusion coefficient, D, and the concentration, C, as a function of position, x. Determination of the diffusion coefficient of the migrating species is essential for the predictions of growth rates, Eq. 9. Fick's first law states that a fixed concentration gradient is required for measuring D. However, this is often difficult to establish experimentally, hence it is generally more convenient to measure the change in concentration of the diffusing species as a function of time, given by Fick's second law, which can be written:

$$\frac{\partial C}{\partial t} = D \frac{\partial^2 C}{\partial x^2} \qquad \text{Eq. 13}$$

Most oxidation processes of metals are governed by the diffusion of metal and/or oxidant. When the initial oxide scale is formed further growth is sustained by either outward transport of metal, and/or inward transport of oxidant. Counter direction diffusion of cations and anions

is commonly found in growing oxide scales, and the parabolic growth rate can be related to the diffusion coefficients [14]:

$$k_{p,t} = \frac{C_0}{b} \int_{pO_2'}^{pO_2''} \left(\frac{Z_M}{|Z_O|} D_M + D_O \right) d \ln p_{O_2} \qquad \text{Eq. 14}$$

The diffusion coefficients of the cations, D_M, and anions, D_O, is thereby of great importance for understanding the oxidation process of the metal. However, this phenomenological relationship does not explain the mechanisms responsible for the diffusion.

The solution of Fick's laws can be modified to represent the explicit experimental parameters [15]. Diffusion coefficients can be determined by various experimental methods, however, the most common procedure is by tracer diffusion experiments using isotopes (*e.g.* ^{54}Cr and ^{18}O) or foreign atoms (*e.g.* Fe and Mn in Cr_2O_3). The distribution of the labeled species in the oxide is measured by depth sensitive elemental characterization techniques such as secondary ion mass spectrometry (SIMS) or electron probe micro-analysis (EPMA).

2.1.4 Internal oxidation

Many metals and alloys are susceptible to *internal oxidation* during high temperature exposures [6,16]. When an oxidant is dissolved in the metal substrate, internal precipitation may occur provided that the internal concentration of the oxidant is sufficient. Internal formation of precipitates is controlled by the volume diffusion of oxidant through the metal matrix, and the penetration of precipitates continues towards the depth of which the concentration of oxidant is too low for continued growth [8]. The concentration of the reactive alloy component is essential for determining whether internal oxidation will occur or not. Wagner proposed a

theoretical model for determining the critical concentration of reactive element in the alloy, $N_B^{(0)}$, at which transition from internal to external oxidation takes place [17]:

$$N_B^{(0)} = \left(g_{BO} \frac{\pi}{2\nu} \frac{V_A}{V_{OX}} \frac{N_O^{(s)} D_O}{D_B} \right)^{1/2} \qquad \text{Eq. 15}$$

g_{BO} is the volume fraction of internal precipitate, ν is the stoichiometric factor, V_A and V_{OX} are the molar volumes of parent metal and precipitate, respectively. Further, $N_O^{(s)}$ is the surface concentration of oxidant, and D_O and D_B are the diffusion coefficients of oxidant and reactive alloy component, respectively.

The growth rate $k_{p,t}$ is in this case based on the rate limiting diffusion of oxidant into the metal and can be expressed by [16]:

$$k_{p,t} = \frac{\varepsilon D_O N_O^{(s)}}{\upsilon N_B^{(0)}} \qquad \text{Eq. 16}$$

where D_O is the diffusion coefficient of oxidant, $N_O^{(s)}$ is the solubility of oxidant at the surface and $N_B^{(0)}$ is the mole fraction of the precipitate forming metal, for instance chromium. ε is a constant describing the blocking effect of precipitates and υ is the stoichiometric factor for the precipitating phase. The condition for validity of Eq. 16 is $D_O N_O^{(s)} >> D_B N_B^{(0)}$.

The model is based on the assumptions that the solubility product, K_{sp}, of the oxidant and precipitate forming metal is vanishingly small, and that the solubility of the two reacting elements is close to zero within the precipitation zone. The remaining metal matrix between the precipitates is depleted of precipitate forming metal, and the diffusion of oxidant is assumed to occur through the metal bulk alone and not being affected by the presence of the

precipitates. As a result of this, the area fraction of precipitate is uniform as a function of depth along the diffusion direction, and zero at the front of the precipitation zone. However, in the case of the formation of internal precipitates with low stability, *e.g.* Cr_2N, K_{sp} will not be infinitesimal, and thereby formation of precipitates will not necessarily occur whenever oxidant is present within the metal. Since N_O decreases as a function of depth, the minimum chromium concentration for sustained precipitation increases. In addition, it has been reported that the formation of internal precipitates provides paths for interfacial oxidant diffusion and thereby accelerates the internal precipitation, further reducing the validity of the classical diffusion predictions for modeling these situations [18]. The lack of complete precipitation will necessarily mean that the volume fraction of precipitates, f_v , varies with depth. This type of situation was analyzed by Ohriner and Morral, and can be adopted to the internal nitridation of chromium bearing alloys, given by the formation of Cr_2N precipitates [9,19,20]. The reaction stoichiometry of the precipitate gives the basis for the solubility product of oxidant and metal in the matrix:

$$K_{sp} = N_{Cr}^{(0)2} N_N^{(s)} \qquad \text{Eq. 17}$$

By assuming that the metal diffusion in the precipitates is insignificant, and that $K_{sp} >> N_N^{(s)3}$, the precipitate fraction, r ,can be expressed by:

$$\frac{\partial r}{\partial t} = \frac{4K_{sp}D_N}{\left(N_{Cr}^{(0)}\right)^3} \frac{\partial}{\partial x}\left[\frac{1}{(1-\alpha r)^2}\frac{\partial r}{\partial t}\right] \qquad \text{Eq. 18}$$

where α is the solubility parameter defined as:

$$\alpha = 1 - \left(\frac{K_{sp}}{N_N^{(s)}} \right)^{1/2} / N_{Cr}^{(0)} \qquad \text{Eq. 19}$$

By utilizing the Boltzmann transformation Eq. 18 can be converted to a differential equation by integration:

$$\frac{(1-\alpha)^2}{(1-\alpha r)^2} = -\frac{N_{Cr}^{(0)}}{8tD_N N_N^{(s)}} \frac{\mathrm{d}x}{\mathrm{d}r} \int_0^{r'} x \, \mathrm{d}r \qquad \text{Eq. 20}$$

This model has proved to describe distribution of internal nitride precipitates in chromium bearing alloys [9,20].

2.1.5 Defect chemistry of Cr_2O_3

Imperfections and defects in the oxide scales enable diffusion. Different types of defects give rise to different diffusion mechanisms. Lattice or point defects in the crystal structure of the oxides are responsible for bulk diffusion. Transport of atoms through bulk may occur either by a vacancy mechanism where an atom in a normal site jumps into a neighboring vacant lattice site, or by an interstitial mechanism where the atom moves from one interstitial site to a neighboring interstitial site. The latter process involves substantial distortion of the lattice and is therefore only likely when the moving atom is smaller than the atoms occupying the normal lattice sites. Knowledge about the defect structure of the oxide is essential to evaluate the migrating elements dominating the oxidation process.

The majority of oxidation experiments in this work have been performed below 1000 °C, and it is therefore most relevant to consider the defect structure of Cr_2O_3 below this temperature. Cr_2O_3 is a p-type semi-conductor at temperatures below 1000 °C [7,21,22]. At the very lowest oxygen partial pressures, there is a changeover to n-type electronic conduction. The most

likely intrinsic ionic majority defects are chromium vacancies, $v_{Cr}^{///}$ and interstitials, $Cr_i^{\bullet\bullet\bullet}$, and minority defects are likely oxygen interstitials, $O_i^{//}$ and vacancies, $v_O^{\bullet\bullet}$. Given that the above mentioned defects dominate concentration-wise, Cr_2O_3 displays the total electroneutrality:

$$3\left[Cr_i^{\bullet\bullet\bullet}\right] + 2\left[v_O^{\bullet\bullet}\right] + p = 3\left[v_{Cr}^{///}\right] + 2\left[O_i^{//}\right] + n \qquad \text{Eq. 21}$$

Oxygen dependency

As Cr_2O_3 in an oxidation experiment is subjected to low oxygen activity near the metal – oxide interface and high oxygen activity at the oxide – gas interface, it is relevant to consider the dominating defect equilibria in Cr_2O_3 under these limiting conditions. At low oxygen activities, undoped Cr_2O_3 is dominated by Cr interstitials and electrons through:

$$2Cr_{Cr}^{\times} + 3O_O^{\times} = 2Cr_i^{\bullet\bullet\bullet} + 6e^{/} + \tfrac{3}{2}\,O_2\,(g) \qquad \text{Eq. 22}$$

and the electroneutrality (Eq. 21) reduces to $3\left[Cr_i^{\bullet\bullet\bullet}\right] = n$. While at the higher oxygen activities however, Cr vacancies and electron holes are likely to dominate:

$$\tfrac{3}{2}\,O_2\,(g) = 2v_{Cr}^{///} + 6h^{\bullet} + 3O_O^{\times} \qquad \text{Eq. 23}$$

and Eq. 21 in this case reduces to $3\left[v_{Cr}^{///}\right] = p$. As illustrated by Eq. 22 and 23, the concentration of all defects in Eq. 21 will be dependent on the oxygen partial pressure, p_{O_2}. The p_{O_2} dependency of the individual defect concentrations may be deduced from the two abovementioned limiting defect situations, in addition to the situation $\left[v_{Cr}^{///}\right] = \left[Cr_i^{\bullet\bullet\bullet}\right]$, which is likely to dominate in the mid-p_{O_2} region, and the equilibrium constants for formation of the ionic defects .

Fig. 2 displays the concentration of all defects in Eq. 21 as function of p_{O_2}. In the inner region of the oxide scale Cr_2O_3 will be an n-type conductor, while towards the outer part of the oxide there will be a gradual change over to a p-type conductor.

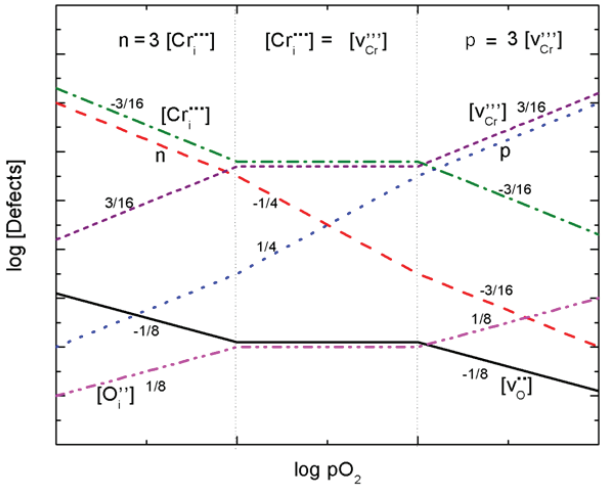

Fig. 2. Brouwer diagram illustrating the defect situation in Cr_2O_3.

During oxidation, the oxygen partial pressure at the metal – oxide interface is equal to the dissociation pressure of the oxide, Eq. 5, while at the oxide – gas interface it is equal to the p_{O_2} of the gas. In a situation where Cr is oxidized in air at 800 °C, the p_{O_2} gradient over the oxide scale will range from 10^{-21} to 0.2. As a result of this large gradient, the concentration of the different defects will vary with the distance between the oxide – gas and oxide – metal interface.

The proposed defect model illustrated in Fig. 2 corresponds well with early studies of chromium self-diffusion in Cr_2O_3 single crystals as a function of p_{O_2} [7,23]. From Wagner's theory $k_p \propto D_{Cr}$ (Eq. 9) and one may, accordingly, expect that the growth rate varies with oxygen partial pressures. The lattice diffusion in chromia is slow, indicating that the

concentration of defects is low in undoped Cr_2O_3 [24]. The correspondence between growth rates and diffusion coefficients reported in literature may therefore have been fortuitous. The relation between diffusion and oxidation rates will be further discussed later.

Dopants

Formation of pure Cr_2O_3 is unlikely to occur during high temperature oxidation of a Cr containing alloy, and various constituents of the alloy may dissolve in the Cr_2O_3 scale. A foreign cation may be treated as a dopant.

Mn is a possible lower valent dopant in Cr_2O_3, a common constituent in chromia forming alloys. At high p_{O_2} dissolution of Mn in Cr_2O_3 may proceed according to:

$$2MnO(s) + \tfrac{1}{2}\,O_2(g) = 2Mn'_{Cr} + 3O^{\times}_{O} + 2h^{\bullet} \qquad \text{Eq. 24}$$

This situation indicates that a lower valent dopant will increase the hole concentration at high oxygen partial pressures.

At low p_{O_2} the dissolution of Mn may be written:

$$2MlO(s) = 2Ml'_{Cr} + v^{\bullet\bullet}_{O} + 2O^{\times}_{O} \qquad \text{Eq. 25}$$

Higher valent dopants such as Ti, will on the other hand increase the concentration of negative defects, notably electrons or Cr vacancies at low and high p_{O_2}, respectively:

$$2MhO_2(s) = 2Mh^{\bullet}_{Cr} + 3O^{\times}_{O} + 2e' + \tfrac{1}{2}\,O_2(g) \qquad \text{Eq. 26}$$

$$3MhO_2(s) = 3Mh^{\bullet}_{Cr} + 6O^{\times}_{O} + v'''_{Cr} \qquad \text{Eq. 27}$$

As the equilibrium concentrations of native defects in Cr_2O_3 are small, extrinsic impurities play an important role in the defect structure Cr_2O_3. It has for instance been concluded that the dominating p-type conductivity encountered at temperatures below 1000 °C is due to compensation of extrinsic acceptor dopants by electron holes [21].

Effects of hydrogen and water

Hydrogen is expected to dissolve in chromia in the form of protons, or more precisely substitutional hydroxide ions on oxygen ion sites. For a p-type conductor this reaction may be written:

$$\tfrac{1}{2}\,H_2\,(g) + O_O^{\times} + h^{\bullet} = OH_O^{\bullet} \qquad \text{Eq. 28}$$

or, in the presence of water vapor:

$$H_2O\,(g) + O_O^{\times} + 2h^{\bullet} = 2OH_O^{\bullet} + \tfrac{1}{2}\,O_2\,(g) \qquad \text{Eq. 29}$$

Both these defect reactions express that introduction of protons in the oxide will decrease the concentration of electron holes, and thereby also the p-type conductivity [21]. Protons may also in principle dissolve by formation of Cr vacancies according to:

$$3H_2O\,(g) + 3O_O^{\times} = 6\,OH_O^{\bullet} + 2v_{Cr}^{'''} \qquad \text{Eq. 30}$$

The total electro neutrality may be written:

$$\left[OH_O^{\bullet}\right] + 2\left[v_O^{\bullet\bullet}\right] + 3\left[Cr_i^{\bullet\bullet\bullet}\right] + p = 3\left[v_{Cr}^{'''}\right] + n \qquad \text{Eq. 33}$$

It is expected that increasing concentration of Cr vacancies increases the cation diffusion through the oxide, and thus also influences the oxidation rate of Cr_2O_3 forming alloys. As a

significant proton concentration would increase the concentration of Cr vacancies, one may suspect a similar effect of water vapor on the oxidation behavior of Cr containing alloys [25,26].

Formation of volatile chromium species

Cr_2O_3 is renowned for the evaporation of volatile chromium species at high p_{O_2} [8,9,27]. Under dry oxidizing conditions, the formation of volatile CrO_3 in metal deficient chromia can be expressed by:

$$Cr_{Cr}^{\times} + \tfrac{3}{2} O_2(g) = v_{Cr}^{'''} + 3h^{\bullet} + CrO_3(g) \qquad \text{Eq. 34}$$

while under wet conditions another volatile species is more likely to be formed:

$$Cr_{Cr}^{\times} + \tfrac{3}{2} O_2(g) + H_2O(g) = v_{Cr}^{'''} + 3h^{\bullet} + CrO_2(OH)_2(g) \qquad \text{Eq. 35}$$

The loss of mass through evaporation promotes cation diffusion, resulting in an increased degradation of the metal substrate. It has been found that the growth kinetics of chromia forming alloys is increased by increasing p_{H_2O} and gas flow [28,29].

Oxidation of Cr

Although pure chromium is not used for practical applications on its own it is widely added as an alloying element to improve corrosion properties of numerous alloys. The oxidation behavior of Cr is therefore of great importance and has been investigated extensively for several decades [6]. By oxidation at high temperatures a scale of Cr_2O_3 is formed. The protective nature of this scale is reflected by a parabolic growth behavior generally found by oxidation above 700 °C at near atmospheric oxygen partial pressures, indicating diffusion controlled oxidation mechanism [7]. Reported parabolic rates differs up to 4 orders of

magnitude, depending on the reaction conditions, sample preparation, surface finish, microstructure of the metal interior, and the formation of volatile chromium species [30,31,32]. The oxidation rate of Cr is dependent on the oxygen pressure of the gas, indicating that the formed scales behave as p- or n-type conductors and that the defect structure influences the growth rates [33,34]. However, the effect of the oxygen pressure may also be a result of variations in the oxide scale microstructure. At reduced oxygen pressures, large stresses and strains are developed within the oxide leading to deformation and cracking of the scale while at high pressures the scales are more adherent and smooth [7,35-37]. The adherence and protective properties of Cr_2O_3 scales have also been found to be influenced by the presence of hydrogen in the metal substrate [38,39]. Furthermore, the adhesion and growth rate of chromia is increased by introducing water vapor to the oxidizing gas [31,40,41].

Although a single phase oxide scale of Cr_2O_3 is formed by oxidation of Cr, it is often found that such scales comprise several layers with different microstructure. This has been attributed to a dissociation process resulting from the failure of the oxide scale to continuously compensate the Cr consumption zone by plastic flow [42]. The oxide scale will crack, and a more porous oxide will form at the metal – oxide interface or within the oxide scale. However, the outward cation diffusion through the inner layer of the scale is still the rate limiting mechanism of the oxidation process.

By oxidation in oxygen rich atmospheres the evaporation of volatile chromium species can be significant [27,43]. Increased velocity of the gas flow, oxygen pressure and water vapor in the oxidizing gas is found to enhance the evaporation rate [31].

Oxidation of Fe-Cr alloys

In the initial *transient* stage of alloy oxidation all available elements, including Cr and Fe, will react with oxygen and form oxides [7,44]. The oxidation process is in this stage governed by the oxide – gas interaction processes, usually following linear kinetics. Eventually, the scale grows in thickness and diffusion of reacting species through the oxide scale becomes the rate limiting represented by parabolic kinetics. The purpose of alloying with Cr is to form a protective Cr_2O_3 scale that limits further oxidation and degradation of the alloy. The process where the oxidation of a solute or alloying element is preferred and forms a continuous scale on the surface of the alloy is referred to as *selective oxidation*. A protective oxide scale formed by selective oxidation is recognized by the oxidation of the least noble constituent of the alloy showing high stability of the oxide phase.

Chromia scales grown on Cr and Fe-Cr alloys show microstructural similarities, indicating that the same oxidation mechanisms predominate the process [7]. The variations in oxidation rates reported for chromia forming Fe-Cr alloys are smaller (about two orders of magnitude) compared to oxidation kinetics of pure Cr [31]. The rate constants are generally found to decrease with increasing Cr content in the alloy [45]. At low Cr contents both Cr_2O_3 and iron oxides, *e.g.* FeO, form on the sample surface and to some extent react into iron chromium spinels, such as $FeCr_2O_4$ [8]. By increasing the Cr concentration a protective Cr_2O_3 scale is formed. However, sustained growth can only be achieved as long as a critical level of Cr content (> ~17 wt.%) is exceeded in the alloy. Most high temperature engineering Fe-Cr alloys are therefore added excess Cr, *i.e.* 20 – 27 wt. %, to ensure formation of continuous layers of chromia [46]. Even at high levels of Cr in the alloy, Fe will dissolve into the oxide scale and diffuse towards the oxide – gas interface. The result is an outer layer of $(Cr, Fe)_3O_4$-spinels or iron oxides [8]. As for pure chromium, the surface of the oxide scales is often

convoluted and wrinkled, in contrast to the "grotesque shapes" formed on pure iron [11]. Features found on the surface such as interfacial cavities and pores often promote cracking and spallation leaving local areas of the metal substrate open, resulting in an enhanced oxidation [7,8]. The formation of volatile chromium species, *e.g.* CrO_3 (g) or $CrO_2(OH)_2$ (g), is also found to increase the oxidation rate by evaporation of the oxide surface [27,28].

Water vapor in the oxidizing gas is generally found to increase the oxidation rate of Fe-Cr alloys, compared to dry conditions [47]. For many alloys initial formation and growth of a protective chromia scale is followed by a significant increase in growth rate. The exact mechanisms responsible for the enhanced rates are not fully understood, although several theories have been suggested. Fujii and Meussner proposed that dissociative transport of oxygen by water in interfacial voids maintained high rates of oxidation of Fe-Cr alloys (Cr ≤ 15 wt.%) in water vapor at 700 – 1100 °C [45,48]. A similar mechanism was suggested by Rahmel and Tobolski, proposing that oxygen transport within interfacial pores is facilitated by a so called H_2/H_2O bridge [49]. Water inside the pores oxidizes the metal at the alloy – oxide interface, while hydrogen reduces the oxide on the outer surface of the void and forms water again. Water vapor has also been suggested to accelerate internal oxidation of Fe-Cr alloys by increasing the solubility of oxygen in the alloy through dissolution of hydrogen in alloys [50,51].

Hydrogen is commonly found in alloys as a result of the fabrication process. The presence of hydrogen in the metal or oxide influences the oxidation behavior, and may alter microstructure, adherence and/or composition of the forming oxide scales [52-55]. As described in an earlier section, hydrogen defects in the oxide scale have been proposed as an explanation for the enhanced oxidation in water containing atmospheres [24-26]. Formation of protonic defects may be compensated by increased concentration of cation vacancies,

accelerating the metal diffusivity. The overall result may be increased growth rate and alterations in the oxide scale composition [53].

Presence of water vapor in the oxidizing gas also significantly increases the evaporation rate from chromia forming alloys [27,28]. By continuously removing chromium from the outer oxide layer by evaporation, the ability to maintain the protective properties of the scale depends on the evaporation rate and the outward flux of chromium from the alloy. The evaporation rate is found to be proportional to the flow rate and water vapor content of the gas. Although the oxidation of the alloy is increased, the mass loss through evaporation may lead to an effective decrease in weight gain and oxide scale thickness of the metal during oxidation, following para-linear kinetics.

If after a certain time the concentration of Cr in the alloy reaches a critical level (< ~17 wt. %) the alloy can no longer re-form a protective scale. Failure of the protective chromia scale may be recognized by the formation of iron oxides, internal oxidation and accelerated oxidation rates [50,56]. This process is termed *breakaway oxidation* and is detrimental for the performance of the alloy. Water vapor in the oxidizing atmosphere has been observed to trigger breakaway oxidation [28,56-58]. It has been suggested that the H_2O (g)/O_2 (g) ratio at the metal – oxide interface is essential for whether breakaway oxidation will occur or not. High levels of H_2O (g), increases the likelihood for triggering breakaway oxidation by increasing the solubility and/or the diffusivity of oxygen in the alloy and thus promoting internal oxidation. Moreover, at sufficiently high p_{O_2} the formation of non-protective Fe rich oxide scales are favored.

To further improve the properties of alloys, minor alloying elements are added. Minor additions (typically 0.2 – 5 wt. %) of selected elements (*e.g.* Al, Mn, Si, Ti) can result in improved oxidation resistance, scale adherence, and/or increased outer spinel formation [7,9,46,59,60]. So called *reactive elements* (*e.g.* Y, La, Ce, Zr) are also reported to have beneficial

effects when added in small amounts (typically 0.1 – 0.2 wt. %) [61-63]. Some of the effects of reactive element additions are; increased selective oxidation of chromium, reduced oxidation rate, increased scale adherence, modifications to the oxide microstructure and the growth processes [61,64,65]. The mechanisms responsible for these effects are not fully understood, although numerous suggestions have been published [64].

Diffusion in oxide scales

Numerous studies have been dedicated to investigate and characterize the diffusion in single and poly crystalline samples of Cr_2O_3, and in thermally grown chromia scales. In an early study of Hagel and Seybolt the self-diffusion of Cr was determined by tracer experiments from 1045 – 1550 °C. Based on the results it was suggested that the rate limiting step of high temperature oxidation of Cr was the volume diffusion of Cr through Cr_2O_3 [66]. This was also the conclusion of Kofstad and Lillerud after comparing the rate of formation of Cr_2O_3, between 800 °C – 1100 °C, with existing data for chromium lattice diffusion [22,66,67]. However, the diffusion coefficients determined in these early studies did not only describe lattice diffusion, but included also contributions from grain boundary diffusion and diffusion through other high diffusivity paths such as pores and micro cracks. This was illustrated in later studies concluding that the chromium lattice diffusion was 4 – 7 orders of magnitude lower than previously determined (1100 – 1570 °C), and that chromium grain boundary diffusion would be the predominating transport mechanism [23,68-71]. A dominating outward cation diffusion should lead to predominant oxide growth at the outer oxide – gas interface, however, a significant fraction of growth has been found to take place at the oxide – metal interface, suggesting that inward diffusion of oxygen also makes a substantial contribution to the oxidation process [38,52,72,73]. In order to clarify the inconsistencies in literature Sabioni *et al.*

performed a comprehensive study of chromium and oxygen diffusion in single and poly crystalline Cr_2O_3 [70,74-76]. They reported that both bulk and grain boundary diffusion of oxygen were faster than the chromium diffusion under the same conditions (1100 – 1300 °C). However, the deviation between oxide growth rates and diffusion coefficients remained unexplained. Tsai *et al.* compared the cation and anion diffusion in massive single and polycrystalline Cr_2O_3 samples with thermally grown oxide scales of the same composition at lower temperatures (800 - 900 °C) [77-79]. Their results showed that the bulk diffusion coefficients of chromium and oxygen were comparable for all three different forms of Cr_2O_3 samples. Interestingly, grain boundary diffusion of both elements was higher in thermally grown scales than in synthesized polycrystals. Further, it was established that chromium diffusivities (especially in grain boundaries) were faster than oxygen. This was in agreement with results from other studies of tracer diffusion [80,81]. By proposing some modifications to the more classical approach of analyzing diffusion profiles by taking the surface roughness into account, Tsai *et al.* found reasonable agreement between calculated (based on diffusion coefficients) and experimentally obtained growth rates of Cr_2O_3 scales. It was concluded that counter current diffusion of chromium and oxygen diffusion, mainly via grain boundaries, maintain growth of chromia scales [78,80,82].

Lobnig *et al.* investigated the diffusion of Cr, Mn, Fe and Ni at 900 °C in thermally grown Cr_2O_3. They found that the lattice diffusion of Mn was about two orders of magnitude higher than for the other cations, and that the diffusion decreased in the order $D_{Mn} > D_{Fe} > D_{Ni} > D_{Cr}$, as also predicted by others [83,84]. This was used to explain the frequently observed formation of an outer $(Cr,Mn)_3O_4$-spinel during oxidation of Mn bearing high-alloy steels, such as ferritic interconnect materials [85,86]. Sabioni *et al.* on the other hand did not find any significant variations in bulk or grain boundary diffusion when comparing Mn and Cr (700 – 1100 °C) [87]. They suggested that MnO and Cr_2O_3 form simultaneously during the initial stage

of oxidation. Due to the minor amounts of Mn in the steel and the high stability of chromia further growth is expected to be dominated by formation of Cr_2O_3. The growth of the outer $(Cr,Mn)_3O_4$-spinel layer was then attributed to the diffusion of Mn at similar rates as Cr through the inner Cr_2O_3. Moreover, Gilewicz-Wolter *et al.* found that Mn was the fastest diffusing cation, compared to Cr and Fe, through $MnCr_2O_4$ (800 – 900 °C), resulting in further accumulation of Mn in the outer region of the spinel phase [88].

The formation of multilayered oxide scales on commercial alloys such as interconnects also influences the oxygen transport. Horita *et al.* reported that the oxygen diffusion in thermally grown oxides on complex SOFC interconnect alloys is faster than in Cr_2O_3 and about two orders of magnitude higher than the growth rates of the oxide scale [89,90]. This discrepancy between growth rates and diffusion coefficients remains unaccounted for although several explanations have been proposed.

Thermal nitridation of chromium bearing alloys

Many metals and alloys are susceptible to corrosion by nitridation during high temperature exposure in nitrogen containing atmospheres. During nitridation both internal and external metal nitride phases are possible, *e.g.* Cr_2N or CrN [9]. Nitridation is a widely used technique for hardening of steels, and to improve wear and corrosion resistance [46,91]. Surface coatings of CrN_x or thermal exposures in nitrogen containing atmospheres can be used to obtain a thin protective layer [92]. Although the chromium nitrides are found to rapidly form into Cr_2O_3 at high temperatures in oxygen containing atmospheres, the high temperature oxidation rate of steels has been found to be reduced by thermal nitridation treatment [93,94]. The formation of dense electrical conducting and corrosion resistant nitrides has also been found to provide a

beneficial effect on the electrical resistance of interconnect materials in fuel cells [95-99]. However, under certain conditions the amount of nitrogen absorbed into the alloy may exceed the solubility limit, resulting in the formation of internal nitride precipitates [46]. This can lead to embrittlement of the alloy. Many industrial processes involve atmospheres containing nitrogen or ammonia, and knowledge of nitridation processes of alloys is therefore of key interest for avoiding premature failure of the metallic equipment. Young *et al.* have investigated the thermal nitridation of various iron and nickel based alloys [18,20,100,101]. They show that the internal nitridation of alloys cannot be described by the Wagner diffusion model of internal oxidation, assuming infinitesimal solubility products and complete reaction between chromium and nitrogen. Due to the low stability of chromium nitrides, the volume fraction of internal nitride precipitates decreases along the diffusion depth of nitrogen into the alloy, and the distribution of precipitates is controlled by the diffusion path of nitrogen, and not nucleation. This means that other theories *e.g.* as proposed by Ohriner and Morral, must be utilized in order to predict the amount of chromium in the alloy required to form external scales rather than internal precipitates [19].

3 Interconnect materials for high temperature solid oxide fuel cells

Purpose and properties

The theoretical output voltage of a fuel cell is given by the electrochemical potential difference between the reacting fuel and oxidant (*e.g.* H_2 and O_2) and the product of these (*e.g.* H_2O). To reach usable voltages, multiple cells are connected in series using interconnects. Interconnects must provide high electrical conductivity while separating the fuel and air and acting as one of the main structural components in the fuel cell assembly. This means that the material used for interconnect must fulfill certain requirements:

- High electrical conductivity at high temperatures
- High chemical and mechanical stability
- Suitable thermal expansion with other fuel cell components
- Gas tightness
- Easy machining and fabrication
- Low cost

While the four first properties may be in focus during the early stages of fuel cell research, the two latter points will play increasingly important roles towards commercialization.

Materials

Many materials have been proposed as possible interconnects for high temperature fuel cells. Ceramic and metallic materials represent the two main potential materials families and have been investigated for decades. A short literature survey of the most essential materials in interconnect research is given in the following.

3.1.1 Ceramic interconnect materials

For several decades the operating temperature of SOFCs was above 1000 °C. At such high temperatures metallic materials are inapplicable for several reasons. This led to the consideration of various ceramic candidate materials for interconnecting purposes. The most widely investigated ceramics were perovskites, holding high electronic and low ionic conductivity. Only a few candidates could meet the severe demands, and among these lanthanum chromites received the most attention. Pure $LaCrO_3$ does not hold sufficiently high electronic conductivity, hence various dopants were utilized. Under oxidizing conditions acceptor doping the material by using *e.g.* Ca and Sr will increase the p-type conductivity [102,103]. Although high electrical conductivities were achieved by utilizing various dopants and by mixing oxide phases *e.g.* Ca doped $LaCrO_3$ and Sm doped CeO_2, some challenges remained unsolved for the ceramic interconnects. The brittle nature, complicated fabrication and high cost are some of the main reasons why these materials are in most cases discarded.

3.1.2 Metallic interconnect materials

Through the decades of extensive research on new and improved materials, and the introduction of anode supported SOFCs the proposed temperature region for SOFC operation has been reduced to ~800 °C. In the case of PCFCs the target working temperature is usually ~650 °C. The lowered operating temperatures enable the use of less complex and costly materials for the interconnect, and various metals and alloys have gained attention as interesting candidates. Some of the first proposed interconnect materials were unalloyed noble metals such as gold, platinum and silver. The latter was regarded as the most probable candidate mostly due to cost, high electrical and thermal conductivity. However, due to the combination of low melting point, and too large TEC silver was discarded [104]. Heat resistant commercial alloys for engineering purposes, *e.g.* Fe-Cr-Al, Ni-Cr-Al, and Co-Cr-Al, could be considered based on their superior oxidation resistance [46]. At high temperature exposures in oxidizing environments these alloys rely on the formation of a protective Al_2O_3 scale. Although, this scale provides excellent protection against corrosion, these alloys are ruled out because of the electrically insulating properties of the oxide [105]. Similar arguments can be used against silica forming alloys. Chromia formers are more susceptible to high temperature corrosion and the oxidation resistance is lower than for alumina and silica formers, however, the electrical conductivity of chromia is orders of magnitude higher than that of alumina and silica [106]. Therefore, two of the most widely used types of alloys for engineering purposes, nickel and iron based chromium bearing alloys came up early in the process, and are still of the most promising metallic interconnect materials [104,107,108].

Extensive research has been invested in nickel based chromium bearing alloys for interconnect purposes [108,109]. These alloys, *e.g.* Haynes 230 and Haynes 242, can offer relatively high electrical conductivity of the oxide scale combined with slow oxidation

kinetics [110-112]. Despite tailoring of the alloy composition to try to meet the interconnect requirements, the thermal expansion of nickel based alloys (15 - 20×10^{-6} /°C) are in general considerably higher than the other fuel cell materials. This makes it nearly impossible to match the other components of the fuel cell, and excludes these materials as interconnect candidates.

Ferritic stainless steels have been considered from the beginning of the search for metallic interconnect materials [104,113]. The low cost and suitable TEC coupled with reasonably good oxidation resistance made this family of alloys tempting alternatives to ceramics and nickel based alloys. During long term exposures the alloy may be depleted of Cr, and the exclusive formation of protective chromia may not be sustained. The amount of chromium in the alloy also influences its thermal expansion coefficient, and can therefore be controlled to match the other fuel cell components [115,116]. As a result of these arguments most ferritic candidate interconnect materials contain 17 – 26 wt.% Cr. Further improvements of the scale adherence and oxidation resistance can be achieved by additions of reactive elements, *e.g.* Y and La, either in metallic form or as oxides (oxide dispersion strengthening, ODS) [61,104,107,117]. Several other elements can also be utilized to tailor the metallurgical properties and the oxidation processes of the alloy [117].

Chromia formers have the disadvantage that volatile chromium species form during oxidation [27,118]. In addition to the increased oxidation rate, oxide and/or oxyhydroxide species of chromium released as gas from the interconnect can migrate into the cathode and react into various chromium containing phases, *e.g.* strontium chromites [119-121]. These phases typically decrease the electrical conductivity of the cathode material, as well as reduce the number of active catalytic sites, resulting in a degradation of the cathode's performance [122]. In order to limit the evaporation, Mn is frequently added in small amounts to the alloy matrix (0.2 – 0.4

wt %). This enables the formation of $(Cr,Mn)_3O_4$-spinel phases in the outer part of the oxide scale [123]. Chromium manganese spinels hold higher electrical conductivities than Cr_2O_3 and improve the total electrical conductivity of the oxide scale.

As a result of the extensive research a ferritic stainless steel was developed specifically for SOFC interconnect application, Crofer 22 APU (ThyssenKrupp VDM) [124]. This is still one of the most widely used interconnect alloys for SOFC. The TEC (~12×10^{-6} /°C) matches that of other fuel cell components. The alloy contains ~22 wt.% Cr to form a protective chromia scale during long term operation, yielding relatively high oxidation resistance [114,125]. Small additions of La improve the oxidation resistance. Further, minor amounts of Mn and Ti are added to form an outer spinel layer, both to reduce the evaporation and to enhance the electrical conductivity of the oxide scale. Titanium additions are also expected to reduce the wrinkling of the oxide. However, some concern has been raised about the high temperature mechanical strength of the alloy. This issue was addressed by the development of the Crofer 22 H, where Nb, W and Si was added to achieve higher creep strength and improved oxidation resistance [126-128]. A similar approach was used by Sandvik Materials Technology when developing the Sanergy HT [129]. This ferritic steel contains similar amounts of Cr and Mn as the two Crofer alloys, resulting in an oxidation behavior recognized by an outer $(Cr,Mn)_3O_4$-spinel layer over a sub layer of Cr_2O_3. Minor amounts of Nb and Mo were added to improve the high temperature strength and oxidation resistance. Nb is often found as precipitations inside the alloy after high temperature exposures forming so called Laves phases. These precipitates have the effect of trapping Si, which will limit the formation of silica and thereby improve the total electrical conductivity [130,131].

The air on the cathode side of a SOFC or PCFC will contain water vapor in various amounts. Water vapor is known to influence the oxidation behavior of chromia formers. It is generally

found that the oxidation rate increases by introducing water vapor [7,132,133]. Changes in microstructure and composition of the oxide scales have also been reported, represented by increased formation of Fe-rich oxides, and internal oxidation [7,28,50,51,134]. Presence of water vapor can also improve scale adherence [123]. An increased Fe concentration in the oxide may have a beneficial effect on the electrical conductivity of the scale [135-137]. Evaporation of chromium species is generally found to increase by increasing water vapor content in the oxidizing gas [28,119]. Mass loss through evaporation can make it difficult to quantitatively determine the effect of water vapor on the oxidation rate [138].

Effects of dual atmosphere environments

The interconnect will be simultaneously exposed to oxidizing conditions (air) on the cathode side and hydrogen containing atmospheres (fuel) on the anode side, the oxygen partial pressures are high enough to form oxides, *i.e.* Cr_2O_3 and $(Cr,Mn)_3O_4$-spinels, in both environments. Investigations of ferritic stainless steels have revealed similar oxidation rates for air and simulated fuel environments [139,140]. Although the same oxide phases are formed in fuel as in air, the microstructure of the oxide scales are changed. The octahedral shaped spinel grains observed in air is replaced by fibrous shaped particles also called whiskers [141].

The permittivity of hydrogen in steel at high temperatures is high and expected to rapidly saturate the alloy [142]. High diffusivity paths, such as grain boundaries in the alloy interior have been suggested to further enhance hydrogen permeation depending on the alloy composition [54,130]. The transport of hydrogen through chromia is slow, hence, when a continuous oxide scale is formed on the anode side of the alloy, further supply of hydrogen during the thermal treatment is limited by the hydrogen permeability of the scales [24,38,143,144].

In so called dual atmosphere environments simulating fuel cell conditions (fuel on the anode side and air on the cathode side) it has been shown that the composition and growth of oxide scales in air when hydrogen is present on the other side of the sample are significantly different from the scales formed in air on both sides [53,54,145-147]. Scales formed in air under dual atmosphere conditions are reported to hold higher concentrations of Fe compared scales formed in air only [145-148]. Moreover, Yang *et al.* found that by introducing water vapor to the air on the cathode side under dual atmosphere conditions, the Fe content in the oxide scales of ferritic stainless steels was further increased [145].

The changes in oxidation behavior under dual atmosphere conditions have been attributed to formation of protonic defects by dissolution of hydrogen in the oxides formed in air [149,150]. Protons may be charge compensated by cation vacancies, leading to an increase in the vacancy concentration and enhanced outward transport of metal ions [26,149,151].

It has also been suggested that the presence of hydrogen may locally depress the p_{O_2} favoring the formation of isolated Fe-rich nodules [54]. One should also be aware that hydrogen may form steam within the oxide scales. If a sufficiently high steam pressure is built up pores may form which may increase the inward oxygen transport and induce faster scale growth [147,152]. This could also result in localized metal attack as observed in association with the Fe-rich nodules.

Furthermore, the extensive growth of iron rich oxides may indicate that dual atmosphere environments increase the risk of breakaway oxidation. The possibility for breakaway oxidation to occur is reported to increase by an increasing water vapor content in the oxidizing gas, and that a high H_2O (g)/O_2 (g) ratio is more likely to trigger breakaway oxidation than a low ratio [50,51,56,153,154]. Breakaway oxidation can in such case be identified by the formation of Fe rich nodules, localized metal loss and internal oxidation.

Coatings

Although strongly influenced by the alloy composition, scale formation is inevitable and the oxide phases formed may not hold sufficiently high electrical conductivity. Further, the evaporation of volatile chromium species resulting in cathode poisoning remains as one of the critical issues for the application of stainless steels as interconnects [122]. It is therefore a broad consensus that coatings are needed in practical applications of stainless steel interconnects. The idea of applying coatings to improve the performance of alloys is not exclusive for the SOFC interconnect research, also in many other applications coatings are used, mostly with the aim of reducing the oxidation rate. However, in the case of interconnect materials other requirements are equally important, including to improve the electrical conductivity and limit chromium evaporation. Although an additional fabrication step is introduced in the manufacturing process the total cost of the interconnect may not be severely increased since less expensive and complex alloys may be utilized provided the coating is protecting the alloy from extensive oxidation.

Various perovskite and spinel oxide coatings have been investigated in the recent years [140,155-168]. Among a wide variety of oxide coatings, Co containing spinels (*e.g.* $(Co,Mn)_3O_4$ and Co_3O_4) have proved to be effective in reducing chromium evaporation, while also providing high electronic conductivity [169]. However, in order to obtain effective blocking of volatile chromium species most of these oxide coatings have been rather thick. This can often result in challenges when it comes to adherence, mechanical stability and sufficiently high electrical conductivity.

Application of thin layers of metallic Co and/or Ce can substantially reduce the corrosion rates and thus increase the lifetime of the fuel cell stack [170]. Furthermore, metallic coatings simplify the manufacturing process as no sintering or annealing is required as for the ceramic

coatings. By oxidation, the Co containing coatings form outer layers of $(Co,Mn)_3O_4$ and Co_3O_4 that are reported to be effective barriers to evaporation and good electrical conductors [168,171]. Metallic coatings are thereby considered as promising candidates for improving the high temperature properties of ferritic interconnect materials.

4 Experimental

This chapter includes materials selection and some of the most important characterization methods. Brief descriptions of the experimental setups and instrumentations used during the work of this thesis are given with the aim of identifying the most important equipment.

Materials selection

The expected low operation temperature of PCFCs enables use of relatively inexpensive interconnect materials such as stainless steels. In this thesis we have been focusing on a newly developed alloy from Sandvik Materials Technology, Sanergy HT. This alloy has been specifically developed as a interconnect material, and tailored to meet the requirements of high temperature fuel cells, *i.e.* SOFC and PCFC.

In addition, another interconnect material, Crofer 22 APU (ThyssenKrupp VDM) was used during nitridation experiments, together with ten model alloys. The compositions of all alloys are listed in Table 1.

Table 1. Chemical composition, wt. %, of alloys used in this study [128,129].

Alloy	Fe	Ni	Cr	Mn	Mo	Nb	Add.
Sanergy HT	Bal.	-	22	0.5	1.0	0.75	Ti
Crofer 22 APU	Bal.	-	22	0.5	-	-	La, Ti
Fe-10Cr	90	-	10	-	-	-	-
Fe-25Cr	75	-	25	-	-	-	-
Fe-35Cr	65	-	35	-	-	-	-
Fe-50Cr	50	-	50	-	-	-	-
Fe-27Ni-10Cr	63	27	10	-	-	-	-
Fe-22Ni-25Cr	53	22	25	-	-	-	-
Ni-10Cr	-	90	10	-	-	-	-
Ni-25Cr	-	75	25	-	-	-	-
Ni-35Cr	-	65	35	-	-	-	-
Ni-50Cr	-	50	50	-	-	-	-

Thin layers of metallic Co and Ce had been applied by a roll-to-roll process during the fabrication. For the coated samples investigated in this study, a single layer of 800 nm Co or a double layer consisting of 10 nm Ce with 800 nm of Co on top were applied.

Experimental setup and instrumentation

4.1.1 Dual atmosphere setup

The sample holder used for dual atmosphere exposures was made from two stainless steel flanges connected to a gas mixer with two separate outlets enabling flow of different gases in each of the individual gas compartments. Samples were mounted in the setup and sealed

mechanically using copper gaskets and bolts, Fig. 3. A high flow of Ar was continuously flushing outside of the experimental setup to decrease degradation of the setup and to avoid any effects of eventual leakages from the reactive gases. Leakages were tested for by pumping vacuum in the two chambers both before and after the oxidation experiments using a rotary pump. Fuel cell conditions were simulated by introducing either wet or dry air on one side (cathode) and 5% H_2 + Ar (wet or dry) on the other side (anode). Serving as a reference, one sample was additionally inserted into each of the two gas compartments and thereby exposed to the same thermal treatment in single atmosphere environments.

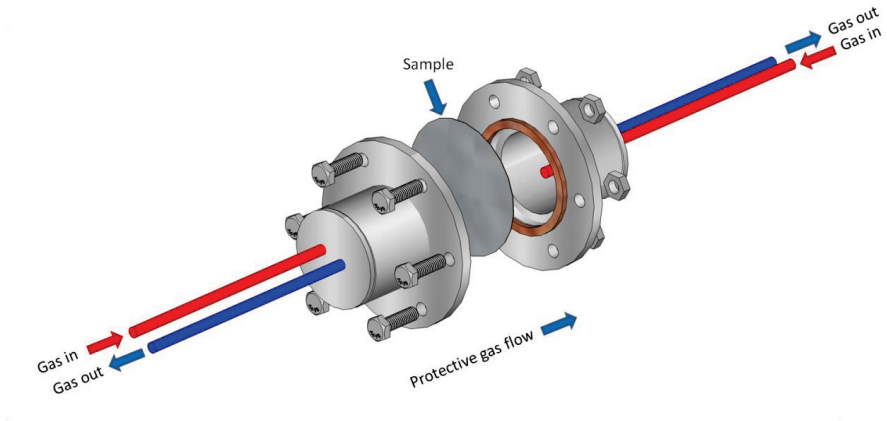

Fig. 3. Schematic illustration of experimental setup for dual atmosphere exposures.

4.1.2 Electrical measurements

Electrical resistance measurements were carried out in a ProboStat measurement cell (NorECs AS). Before each experiment two samples were pre-oxidized in wet air for 24 h at 700 °C, and two gold wires were spot welded on each of the samples. The spot welded electrodes ensure good electrical contact with the samples, eliminating the contact resistance between sample and electrode. Further, Pt ink was painted on one side of each sample before they were

sandwiched together with Pt grid connecting the painted surfaces. The sample assembly was then mounted in the measurement cell. An S-type thermocouple placed next to the samples was connected to a Eurotherm 2216 temperature controller that was used to control the furnace temperature. A constant current was applied and the resulting voltage drop over the interface between the two samples was measured using an Agilent 35210 data acquisition unit with a voltmeter switch module. Contributions to the resistance from the alloy itself and the platinum contact layer were considered negligible. The setup was tested for several currents and the resulting voltage behaved according to Ohm's law indicating that the resistance measured was purely ohmic.

4.1.3 Thermogravimetry

Thermogravimetry is one of most widely used methods in the field of oxidation and corrosion science. The strength of the method is the in-situ measurement of the oxidation rate. The specific instrument used for thermogravimetric measurements in this work was a C.I. Electronics MK2 microbalance with a maximum sensitivity of 10 μg, and a maximum load capacity of 5 g. Both sample and counterweight were suspended from the balance arms using Pt threads. The sample was held in a closed alumina tube inside a vertical tube furnace, and the counterweight was held at room temperature in a glass tube. The gas tight TG setup was connected to a gas mixer controlling the composition and flow of the reaction gas. Due to various sources of noise, the practical sensitivity at high temperatures when measuring in air was ~0.8 mg corresponding to ~0.1 mg/cm^2.

4.1.4 Gas phase analysis

A gas phase analysis apparatus (GPA) was utilized for oxidizing samples in various isotopic oxygen atmospheres. The GPA consists of an enclosed quartz tube used as reaction chamber for the samples, a mass spectrometer and a gas supply system. The samples were inserted into the quartz tube, and a moveable horizontal tube furnace was rolled into position for heating the samples. Rapid heating/cooling was achieved by rolling the furnace back and forth while at high temperatures. The total pressure in the enclosed volume, and the composition of the gas was monitored using a Pfeiffer CMR 261 pressure gauge and a Pfeiffer Prisma QME 200 quadropole mass spectrometer (MS), respectively. The gas supply system enabled use of atmospheres of different oxygen isotopes ($^{18,18}O_2$ and $^{16,16}O_2$).

4.1.5 Gas mixer

For controlling the atmosphere during heat treatment of the samples, in-house built gas mixers were used. Although slightly different design of the different gas mixers, the basic working principles were the same. The gas flow is controlled by several rotameters (Brooks Instruments Sho-Rate 1355). Bubblers filled with di-buthylphtalate are connected to the flowmeters to create a small overpressure through the various parts of the gas mixer and finally over the samples. A column containing P_2O_5 is used as a drying stage for the gas giving a $p_{H_2O} \sim 10^{-5}$ atm. Water vapor is introduced by passing the gas through a saturated solution of KBr and water, resulting in a $p_{H_2O} \sim 0.025$ atm at 25 °C.

Materials characterization

4.1.6 Scanning electron microscope

All micro structural characterizations of the samples in this work were carried out using a FEI Quanta 200 F scanning electron microscope (SEM) equipped with a field emission gun (FEG). The instrument is a so called environmental SEM (ESEM) that can operate at chamber gas pressures between 10^{-4} Pa and 4000 Pa. This enables imaging of samples with low electronic conductivity without further sample preparation, *e.g.* by applying conductive coatings. The SEM was equipped with an Everhart-Thornley detector (ETD) for detecting secondary electrons at high vacuum mode, and a large field detector (LFD) for low vacuum. A solid-state backscatter detector, SSD-BSD, was used for phase contrast imaging by backscattered electrons. The SEM was, moreover, equipped with an energy dispersive X-ray spectrometer (EDS, EDAX Pegasus 2200). The EDS detects characteristic X-ray radiation, and is used for semi quantitative elemental analysis of the samples.

Cross sections were also characterized by electron back scattered diffraction (EBSD, EDAX OIM Analysis System with a CD-200 Nordiff camera). This technique was used for mapping of crystallographic orientation.

4.1.7 Secondary ion mass spectrometer

Characterization of oxygen isotope distribution in oxide scales was carried out by secondary ion mass spectrometer (SIMS) using a Cameca IMS 7f instrument with a primary beam of 15 keV Cs^+ ions. Concentration profiles of ^{16}O and ^{18}O were recorded versus depth. The depth of the sputtered craters was measured with a profilometer (Dektak 8 stylus). For depth calibration a constant erosion rate was assumed. The rastering area was 200×200 μm, while the area of detection was a centered 70×70 μm area.

4.1.8 X-ray diffraction

In order to investigate the phases present on the heat treated metal samples X-ray diffraction (XRD) was used. Three different instruments were utilized; for the samples treated at UiO a Siemens D5000 was used as a routine instrument until it was replaced by a Bruker D8 Advance, while a Philips X'pert Pro was used to analyze the nitrided surfaces of samples fabricated at UNSW.

4.1.9 Dilatometry

Thermal expansion measurements were carried out using a Netzsch DIL 402C dilatometer. The instrument utilizes the displacement of a horizontal pushrod to determine the linear dilation of the sample as a function of temperature. Measurements were carried out in dry nitrogen atmosphere in order to limit the oxidation of alloy samples. The instrument has a resolution of 0.125 nm at 500 μm measuring range, and the temperature accuracy for the S-type thermocouple used is ±1 °C up to 1000 °C.

5 Papers and manuscripts

PAPER I *Sandvik Sanergy HT - A potential interconnect material for $LaNbO_4$–based proton ceramic fuel cells*

Skilbred, A. W. B.; Haugsrud, R. *J. Power Sources* **2012**, *206, 70.*

PAPER II *Investigations of oxidation mechanisms and oxygen diffusion in oxide scales grown on coated and uncoated interconnect material for solid oxide fuel cells*

Skilbred, A. W. B.; Haugsrud, R. *To be submitted.*

PAPER III *The effect of dual atmosphere conditions on the corrosion of Sandvik Sanergy HT*

Skilbred, A. W. B.; Haugsrud, R. *Int. J. Hydrogen Ener.* **2012***, 37, 8095.*

PAPER IV *The effect of water vapour on the corrosion of Sandvik Sanergy HT under dual atmosphere conditions*

Skilbred, A. W. B.; Haugsrud, R. *Oxid. Met.* Published online: 06 October **2012**, DOI: 10.1007/s11085-012-9313-7

MANUSCRIPT A *Thermal nitridation of iron and nickel based chromium holding alloys*

Skilbred, A. W. B.; Norby, T.; Zhang, J.; Young, D. J. *To be submitted.*

PAPER I:

Sandvik Sanergy HT – A potential interconnect material for $LaNbO_4$-based proton ceramic fuel cells

Skilbred, A. W. B.; Haugsrud, R. *J. Power Sources* **2012**, *206, 70.*

PAPER II:

Investigations of oxidation mechanisms and oxygen diffusion in oxide scales grown on coated and uncoated interconnect material for solid oxide fuel cells

Skilbred, A.W. B; Haugsrud, R. *To be submitted.*

PAPER III:

The effect of dual atmosphere conditions on the corrosion of Sandvik Sanergy HT

Skilbred, A. W. B.; Haugsrud, R. *Int. J. Hydrogen Energ.* **2012***, 37, 8095.*

PAPER IV:

The effect of water vapour on the corrosion of Sandvik Sanergy HT under dual atmosphere conditions

Skilbred, A. W. B.; Haugsrud, R. *Oxid. Met.* Published online: 06 October **2012**, DOI: 10.1007/s11085-012-9313-7

MANUSCRIPT A:

Thermal nitridation of iron and nickel based chromium bearing alloys

Skilbred, A. W. B.; Norby, T.; Zhang, J.; Young, D. J. *To be submitted.*

6 Summarizing discussion

The papers presented have addressed various aspects regarding the high temperature properties of interconnect materials for SOFC and PCFC. A relatively newly developed ferritic stainless steel Sandvik Sanergy HT was, after careful materials selection, chosen as a promising candidate. Since little information about the high temperature properties of the Sanergy HT was found in literature, it was decided to investigate the material thoroughly, focusing on its performance under PCFC conditions. In PAPER I an overview of key high temperature properties of the material is given, revealing the overall features of the oxidation process under various conditions. Further characterization of the oxidation is presented in PAPER II, focusing on the diffusion of oxygen ions and cations to reveal the mechanisms governing the oxidation process. PAPER III and IV address key aspects of the oxidation behavior of Sanergy HT under simulated fuel cell dual atmosphere conditions. The effect of dual atmosphere exposures was clear, recognized by the formation of Fe rich oxide nodules accompanied by localized metal loss. It is suggested that the Sanergy HT may have to be improved by coatings in order to meet the requirements of long term operation in a fuel cell. PAPER III and IV presents some results on the oxidation behavior of Sanergy HT where a double layered metallic coating of 10 nm Ce and 800 nm Co had been applied. Another possible method for improving the oxidation resistance and mechanical properties of steels is thermal nitridation. This was also suggested utilized in the case of interconnects for PCFC. PAPER V presents a study performed to research the thermal nitridation of various steels, including two commercial ferritic interconnect steels. It was found that the amount and depth of internal Cr_2N precipitates increased with increasing Cr content, attributed to formation of high diffusivity paths for nitrogen along metal–nitride interfaces.

The aim of this chapter is to take the discussions in PAPER I – IV further, and to link the individual works.

Oxidation behavior of Sanergy HT

The oxidation of Sanergy HT at high temperatures in single air atmospheres follows parabolic kinetics, indicating that the oxidation is governed by diffusion of reacting species through the forming oxide scale. This is commonly found for chromia and alumina formers. It is assumed that outward diffusion of cations is the rate limiting step during oxidation of these types of alloys. However, by screening the literature on diffusion properties of Cr_2O_3 the domination of growth in the favor of cation diffusion is not so obvious.

During the oxidation of Sanergy HT, and other Cr and Mn bearing alloys, the oxide scale comprises an inner layer of Cr_2O_3 and an outer layer of $(Cr,Mn)_3O_4$ spinel. By two stage oxidation we found that the predominant oxide growth occurs in the outer region near the oxide – gas surface, which is a good indication that outward transport of cations is the predominant process of the oxidation. However, in this study the two stage oxygen isotope profiling by SIMS was performed on samples oxidized for a relatively short period of time, and the outer spinel layer was thin compared to the chromia layer. Our results show that by extending the oxidation time, and thereby also increasing both the total and relative thickness of the outer spinel, the (^{18}O and ^{16}O) isotope distribution profiles were remarkably different and indicated almost complete exchange in the outer oxide scale (close to equal concentrations of the two isotopes). Close to the metal – oxide interface insignificant exchange had occurred (meaning that one of the isotopes (^{16}O) was only found in small amounts).

Both in the work presented in this thesis (PAPER II) and in literature, rather high oxygen diffusion coefficients are found in thermally grown oxide scales compared to what is expected based on studies of the oxidation mechanism. Rapid gas exchange and oxygen diffusion in the spinel phase is also indicated by the slightly "S-shaped" diffusion profiles at higher temperatures (900 °C). Based on the depth of the SIMS profiling we found that the obtained diffusion profiles presented in PAPER II are mainly representing the oxygen ion diffusion in the outer $(Cr,Mn)_3O_4$-spinel layer. Indicating that the effective oxygen diffusion through the outer spinel phase may be higher than through the inner chromia layer, and that the transport of oxygen may play a more pronounced role in the oxidation process than expected. This means that a significant fraction of oxide growth occurs inside the oxide scale, close to the interface between the spinel and chromia. And that the outward cation transport through the inner Cr_2O_3 is the rate limiting mechanism. Mrowec *et al.* have proposed a similar mechanisms to account for the formation of multiple layered single phase oxide scales frequently found for *e.g.* chromia formers [42].

The effective oxygen diffusion measured also includes transport through high diffusivity paths *e.g.* grain boundaries, and transport through micro cracks and pores, the measured effective oxygen diffusion may therefore be substantially higher than the bulk diffusion coefficient.

Based on the results from both oxidation studies (including isotopic two stage oxidation) and the oxygen diffusion profiles we propose that the oxidation process can be separated into several stages with respect to time, Fig. 5. The rate and duration of the separate stages depend on the temperature and atmosphere. The figure also includes schematics illustrating SIMS profiles resulting from the separate stages of oxidation. In the initial stage (stage 1), transient oxidation occurs and a thin oxide scale is established where the composition reflects

essentially the composition of the alloy. This is followed by the formation of a protective Cr_2O_3 scale (stage 2) and further growth is governed by the outward diffusion of cations. Growth occurs at the oxide – gas surface, and inward oxygen transport is negligible. The next stage is identified by predominant growth of the $(Cr,Mn)_3O_4$ and Cr_2O_3 in the outer part of the oxide scale (stage 3). This is given by the rather fast inward oxygen diffusion in the outer oxide layer, we suggest that a considerable fraction of oxide growth occurs within the oxide near the Cr_2O_3 – $(Cr,Mn)_3O_4$-spinel interface. However, the outward cation diffusion through the inner Cr_2O_3 layer is still the rate limiting mechanism.

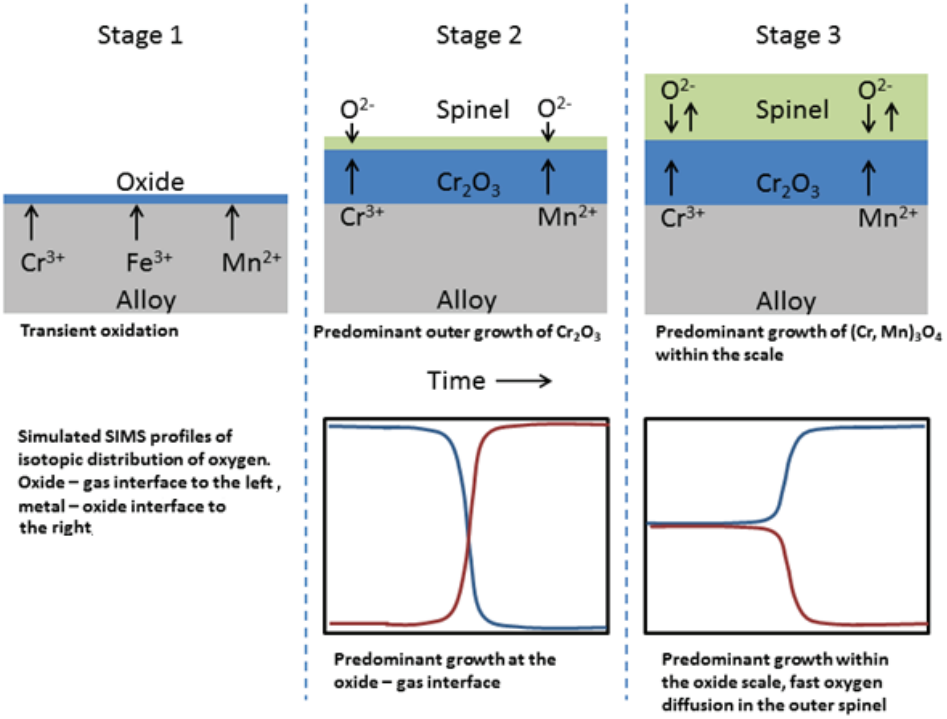

Fig. 4 Proposed oxide scale growth and resulting SIMS profiles after two stage oxidation experiments.

A last stage of accelerated oxidation may take place after a certain time period, depending on the temperature, as found in PAPER I.

Oxidation under dual atmosphere conditions

Over the last decade infrequent reports have been published on the effect of dual atmosphere environments and its influence on the high temperature oxidation on the air side of interconnect materials [55,145,147]. In comparison with the vast number of papers presenting oxidation and corrosion of interconnect materials under single atmosphere conditions it may be suggested that the effect of dual atmospheres is underrated in the scientific community. As PAPER III and PAPER IV show, the most significant effect of dual atmosphere environments compared to oxidation under single air conditions is an extensive formation of Fe rich oxide nodules, accompanied by localized metal loss. There are several mechanisms proposed in literature to be responsible for the dual atmosphere effect. However, no clear conclusions have been given. We believe that the dual atmosphere effect on the oxidation in air is a result of several contributing and cooperating mechanisms.

It has previously been reported that the transport of hydrogen in steels is fast, and hence a thin sample is likely to be saturated within the initial stage of exposures before a protective oxide scale is formed [142]. The hydrogen diffusion in Cr_2O_3 on the other hand is very slow. It can therefore be expected that the hydrogen transport from the fuel to the air side through the sample is limited after a protective oxide scale is formed. In the case of chromia forming alloys such as Sanergy HT, the initial stage of oxidation (prior to the establishment of a protective scale) at high temperatures is short. However, based on the assumption that the steel sample is saturated with hydrogen within the first few minutes of high temperature exposures it is suggested in literature that the thermodynamic conditions of the surface may

be altered, resulting in a more favored formation of Fe rich oxides together with the expected growth of Cr_2O_3 [54,172].

An interesting observation in PAPER IV is that the formation of Fe rich nodules is not randomly distributed over the sample surface, but aligned and elongated in a certain preferred orientation. Additional results (by EBSD) further indicated that the nodule formation was independent on the alloy interior, contradicting previous assumptions in literature that the preferred localization of nodule formation would be related to high diffusivity paths, such as grain boundaries [54]. This seems reasonable when considering the fast transport of hydrogen through steel, which would be expected to lead to a nearly even distribution of hydrogen throughout the alloy. High diffusivity paths are therefore not expected to have any significant effect since the alloy may already be saturated with hydrogen. We suggest that the localization of nodule formation is related to the surface deformations of the as received samples resulting from the cold work during fabrication, *e.g.* rolling process. Surface defects and deformations are known to influence the oxidation behavior of alloys, and could serve as a trigger for nodule formation. Further, it seems that in the case of Sanergy HT the presence of surface deformations has no significant effect on the oxidation process under single atmosphere conditions.

Alterations to the defect chemistry in the oxide scale induced by the hydrogen species present have been proposed in literature to change the oxidation behavior that could contribute to the formation of Fe rich oxide phases [25,26]. This is explained by a defect chemistry model showing that an increased concentration of protons (associated with an oxide ion as hydroxide species) will increase the concentration of metal vacancies in the oxide scale close to the metal – oxide interface (low p_{O_2}). The increasing number of metal vacancies is likely to enhance the outward transport of metal species, *e.g.* Cr, Mn and/or Fe. This may be a contributing factor

to the anomalous oxidation behavior observed under dual atmosphere conditions, however, as the cation volume diffusion is expected to be low any substantial alterations to the oxide scale is likely to origin from a faster and more pronounced process than a slight increase in cation diffusion.

Further, growth stresses are known to influence the scaling mechanisms [173]. Different starting thicknesses of high Cr has been suggested to induce different levels of stress between the oxides and alloys may samples [114]. Hence, the change in growth rates of the chromia base scales may be the result of compressive growth stresses in the scales which can relax by plastic deformation of the substrate for thin specimens [174]. Varying sample thicknesses are found to result in changes in oxide scale composition and microstructure that resembling the formation of Fe enriched oxide scales observed under dual atmosphere conditions. Furthermore, alterations and build-up of growth stresses by surface defects may induce similar effects, explaining the observed relation between the formation of Fe rich oxide nodules and surface roughness left by cold work during fabrication.

Breakaway oxidation is a process that involves alterations of the oxidation behavior. Essuman *et al*. found that increasing water vapor in the oxidizing gas (single atmosphere) promoted breakaway oxidation [50,153]. They proposed that the formation of Fe-rich oxides during breakaway oxidation is a result of internal oxidation. We suggest that similar mechanisms are responsible for dual atmosphere effect identified by extensive formation of Fe-rich nodules. The hydrogen supplied by transport through the interconnect under dual atmosphere conditions increases the concentration of water vapor at the metal – oxide interface, leading to substantial metal loss, internal oxidation and breakaway oxidation resulting in nodules. By also introducing water vapor in the oxidizing gas (air) this process is further enhanced. This is in accordance with literature where it is proposed that in gas mixtures of H_2O (g) and O_2 (g)

the competitive adsorption of water or oxygen molecules at the metal surface governs whether breakaway oxidation occurs or not [154]. It is therefore suggested that the H_2O (g)/ O_2 (g) ratio is crucial for the initiation of breakaway oxidation, and that an increased level of H_2O (g) will increase the chance of breakaway.

Evaporation of volatile chromium species (especially under wet conditions) has been proposed as a reason for triggering breakaway oxidation since the supply of Cr may not be sufficient to compensate for the loss of metal both by evaporation and oxide formation. This may be one of the reasons why we did not observe any evidence of breakaway oxidation of interconnect samples coated with Ce and Co. These coatings are reported to significantly reduce evaporation [170,171]. However, the lack of dual atmosphere effects on coated samples may also a result of other processes, *e.g.* by the inhibiting effect of ceria on breakaway oxidation [56].

Based on our findings and the available literature we propose that the effect of dual atmosphere conditions on the oxidation of Sanergy HT is a result of several contributing processes. The high concentrations of hydrogen at the metal – oxide interface may change the thermodynamic conditions favoring the formation of Fe-rich oxides. Furthermore, the hydrogen present may lead to an increased outward cation transport due to alteration in the defect chemistry of the oxide scale. However, these two mechanisms are considered to be minor contributions to the anomalous oxidation occurring. We propose that the high concentration of water vapor present at the metal – oxide interface and in the oxide scale, resulting from the hydrogen transported through the sample and from the water vapor in the atmosphere in combination of relaxation of growth stresses are responsible for the breakaway type of oxidation identified by formation of Fe-rich nodules accompanied by localized metal

loss. The surface deformations left from the cold work of the samples act as trigger points for this anomalous oxidation behavior.

Sandvik Sanergy HT; a possible PCFC interconnect?

Based on the TEC and ASR values found in this thesis the Sandvik Sanergy HT may be a suitable interconnect material for PCFC, depending on the materials used in the fuel cell assembly. The alloy shows good oxidation resistance, especially at lower temperatures (700 - 800 °C), and the phases in the oxide scale are identified as fairly good electrical conductors (~6 $m\Omega cm^2$ at 700 °). Based on the oxidation rates measured in air it is predicted that the lifetime of the interconnect far exceeds the expected lifetime of the fuel cell (>50 000 h). Although, the influence of dual atmosphere conditions on the oxidation behavior is significant, and generates uncertainties to how this material will perform under operation in a fuel cell, it is likely that the oxide growth kinetics is so slow at the expected working temperature of a PCFC (600 – 700 °C) that the influence of dual atmosphere will not produce any significant effects on the performance of the material. In an SOFC, on the other hand, the temperature will be higher (750 – 850 °C), and the dual atmosphere effect can pose a threat to the performance of the interconnect. Further, as pointed out in this thesis the water vapor content and the composition of the fuel and oxidant atmosphere is of great importance with regards to the extent of the dual atmosphere effect. The application of metallic Ce and Co coatings is regarded as a beneficial and likely improvement of performance of the Sanergy HT, both with respect to limited chromium evaporation and reduced negative effects of dual atmosphere.

References

(1) *International Energy Outlook 2006*, **2006**.

(2) Stern, N.; *Stern Review: The Economics of Climate Change*, Cabinet Office - HM Treasury, **2007**.

(3) Kreuer, K. D. *Solid State Ionics* **1997**, *97*, 1.

(4) Kreuer, K. D. *Ann. Rev. Mater. Res.* **2003**, *33*, 333.

(5) Haugsrud, R.; Norby, T. *Solid State Ionics* **2006**, *177*, 1129.

(6) Kofstad, P. *High-Temperature Oxidation of Metals*; Wiley, **1967.**

(7) Kofstad, P. *High temperature corrosion*; Elsevier Applied Science, **1988**.

(8) Birks, N.; Meier, G. H. *Introduction to High Temperature Oxidation of Metals*; Edward Arnold Publishers, Ltd, **1983**.

(9) Young, D. J. *High Temperature Oxidation and Corrosion of Metals*; Elsevier, **2008**; Vol. 1.

(10) Ellingham, H. J. T. *J. Soc. Chem. Ind., London* **1944**, *63*, 125.

(11) Pilling, N. B.; Bedworth, R. E. *J. Inst. Metals* **1923**, 54.

(12) Brylewski, T.; Dąbek, J.; Przybylski, K. *J. Therm. Anal. Calorim.* **2004**, *77*, 207.

(13) Wagner, C. *Z. Physik. Chem.* **1933**, *B21*, 25.

(14) Atkinson, A. *Rev. Mod. Phys.* **1985**, *57*, 437.

(15) Crank, J. *The Mathematics of Diffusion. 2nd Ed*; Oxford Univ. Press, **1975**.

(16) Rapp, R. A. *Corrosion (Houston, TX, U. S.)* **1965**, *21*, 382.

(17) Wagner, C. *Z. Elektrochem. Angew. Phys. Chem.* **1959**, *63*, 772.

(18) Tjokro, K.; Young, D. J. *Oxid. Met.***1995**, *44*, 453.

(19) Ohriner, E. K.; Morral, J. E. *Scripta Metall.* **1979**, *13*, 7.

(20) Udyavar, M.; Young, D. J. *Corros. Sci.* **2000**, *42*, 861.

(21) Holt, A.; Kofstad, P. *Solid State Ionics* **1994**, *69*, 137.

(22) Kofstad, P.; Lillerud, K. P. *J. Electrochem. Soc.* **1980**, *127*, 2410.

(23) Hoshino, K.; Peterson, N. L. *J. Am. Ceram. Soc.* **1983**, *66*, C202.

(24) Kofstad, P. *Oxid. Met.* **1995**, *44*, 3.

(25) Norby, T. *Adv. Ceram.* **1987**, *23*, 107.

(26) Norby, T. *J. Phys. IV* **1993**, *3*, 99.

(27) Caplan, D.; Cohen, M. *J. Electrochem. Soc.* **1961**, *108*, 438.

(28) Asteman, H.; Svensson, J. E.; Norell, M.; Johansson, L. G. *Oxid. Met.* **2000**, *54*, 11.

(29) Young, D.; Pint, B. *Oxid. Met.* **2006**, *66*, 137.

(30) Caplan, D.; Harvey, A.; Cohen, M. *J. Electrochem. Soc.* **1961**, *108*, 134.

(31) Hindam, H.; Whittle, D. P. *Oxid. Met.* **1982**, *18*, 245.

(32) Caplan, D.; Sproule, G. I. *Oxid. Met.* **1975**, *9*, 459.

(33) Lillerud, K. P.; Kofstad, P. *J. Electrochem. Soc.* **1980**, *127*, 2397.

(34) Young, D. J.; Cohen, M. *J. Electrochem. Soc.* **1977**, *124*, 775.

(35) Lillerud, K. P.; Kofstad, P. *Oxid. Met.* **1982**, *17*, 195.

(36) Kofstad, P.; Lillerud, K. P. *Oxid. Met.* **1982**, *17*, 177.

(37) Lillerud, K. P.; Kofstad, P. *Oxid. Met.* **1982**, *17*, 127.

(38) Tveten, B.; Hultquist, G.; Norby, T. *Oxid. Met.* **1999**, *51*, 221.

(39) Tveten, B.; Hultquist, G.; Wallinder, D. *Oxid. Met.* **2001**, *55*, 279.

(40) Hultquist, G.; Tveten, B.; Hornlund, E. *Oxid. Met.* **2000**, *54*, 1.

(41) Haensel, M.; Quadakkers, W. J.; Young, D. J. *Oxid. Met.* **2003**, *59*, 285.

(42) Mrowec, S. *High Temp. Mater. Proc.* **2005**, *24*, 375

(43) Gulbransen, E. A.; Andrew, K. F. *J. Electrochem. Soc.* **1957**, *104*, 334.

(44) Chattopadhyay, B.; Wood, G. C. *Oxid. Met.***1970**, *2*, 373.

(45) Fujii, C. T.; Meussner, R. A. *J. Electrochem. Soc.* **1964**, *111*, 1215.

(46) Lai, G. Y. *High Temperature Corrosion of Engineering Alloys*; ASM International, **1990**.

(47) S.R.J. Saunders, M. M., F. Rizzo *Prog. Mater. Sci.* **2008**, *53*, 775.

(48) Fujii, C. T.; Meussner, R. A. *J. Electrochem. Soc.* **1963**, *110*, 1195.

(49) Rahmel, A.; Tobolski, J. *Corros. Sci.* **1965**, *5*, 333.

(50) Essuman, E.; Meier, G. H.; Zurek, J.; Haensel, M.; Quadakkers, W. J. *Oxid. Met.* **2008**, *69*, 143.

(51) Essuman, E.; Meier, G. H.; Zurek, J.; Haensel, M.; Singheiser, L.; Quadakkers, W. J. *Mater. Sci. Forum* **2008**, *595-598*, 699.

(52) Hultquist, G.; Tveten, B.; Hornlund, E.; Limback, M.; Haugsrud, R. *Oxid. Met.* **2001**, *56*, 313.

(53) Zhenguo, Y.; Walker, M. S.; Singh, P.; Stevenson, J. W.; Norby, T. *J. Electrochem. Soc.* **2004**, *151*, B669.

(54) Rufner, J.; Gannon, P.; White, P.; Deibert, M.; Teintze, S.; Smith, R.; Chen, H. *Int. J. Hydrogen Energ.* **2008**, *33*, 1392.

(55) Ziomek-Moroz, M.; Covino, B. D., Jr.; Cramer, S. D.; Holcomb, G. R.; Bullard, S. J.; Singh, P.; Windisch, C. F., Jr. In *29th International Technical Conference on Coal Utilization & Fuel Systems*; Coal Technology Association: 2004; Vol. 2, p 1121.

(56) Jianian, S.; Longjiang, Z.; Tiefan, L. *Oxid. Met.* **1997**, *48*, 345.

(57) Othman, N. K.; Zhang, J.; Young, D. J. *Mater. Corros.* **2011**, *62*, 496.

(58) Pujilaksono, B.; Jonsson, T.; Heidari, H.; Halvarsson, M.; Svensson, J. E.; Johansson, L. G. *Oxid. Met.* **2011**, *75*, 183.

(59) Giggins, C. S.; Pettit, F. S. *J. Electrochem. Soc.* **1971**, *118*, 1782.

(60) Stott, F. H.; Wood, G. C.; Stringer, J. *Oxid. Met.* **1995**, *44*, 113.

(61) Whittle, D. P.; Stringer, J. *Philos. T. Roy. Soc. A* **1980**, *295*.

(62) Wallwork, G. R. *Rep. Prog. Phys.* **1976**, *39*.

(63) Cotell, C. M.; Yurek, G. J.; Hussey, R. J.; Mitchell, D. F.; Graham, M. J. *Oxid. Met.* **1990**, *34*, 173.

(64) Hou, P. Y.; Stringer, J. *Mater. Sci. Eng. A* **1995**, *202*, 1.

(65) Hussey, R. J.; Graham, M. J. *Oxid. Met.* **1996**, *45*, 349.

(66) Hagel, W. C.; Seybolt, A. U. *J. Electrochem. Soc.* **1961**, *108*, 1146.

(67) Lillerud, K. P.; Kofstad, P. *J. Electrochem. Soc.* **1980**, *127*, 2397.

(68) Atkinson, A.; Taylor, R. I. *NATO ASI Ser., Ser. B* **1985**, *129*, 285.

(69) Atkinson, H. V. *Oxid. Met.* **1985**, *24*, 177.

(70) Sabioni, A. C. S.; Lesage, B.; Huntz, A. M.; Pivin, J. C.; Monty, C. *Philos. Mag. A* **1992**, *66*, 333.

(71) Sabioni, A. C. S.; Huntz, A. M.; Millot, F.; Monty, C. *Philos. Mag. A* **1992**, *66*, 361.

(72) Tveten, B. N. *PhD thesis*, **2000**.

(73) Graham, M. J.; Eldrige, J. I.; Mitchell, D. F.; Hussey, R. J. *Mater. Sci. Forum* **1989**, *43*, 207.

(74) Sabioni, A. C. S.; Huntz, A. M.; Philibert, J.; Lesage, B.; Monty, C. *J. Mater. Sci.* **1992**, *27*, 4782.

(75) Sabioni, A. C. S.; Huntz, A. M.; Millot, F.; Monty, C. *Philos. Mag. A* **1992**, *66*, 351.

(76) Sabioni, A. C. S.; Huntz, A. M.; Millot, F.; Monty, C. *Philos. Mag. A* **1992**, *66*, 361.

(77) Tsai, S. C.; Huntz, A. M.; Dolin, C.; Monty, C. *Mikrochim. Acta, Suppl.* **1996**, *13*, 587.

(78) Tsai, S. C.; Huntz, A. M.; Dolin, C. *Oxid. Met.* **1995**, *43*, 581.

(79) Tsai, S.; Tsai *Mater. Sci. Eng. A* **1996**, *A212*, 6.

(80) Tsai, S. C.; Huntz, A. M.; Dolin, C. *Mater. Sci. Eng. A* **1996**, *A212*, 6.

(81) Huntz, A. M.; Balmain, J.; Tsaï, S. C.; Messaoudi, K.; Loudjani, M. K.; Lesage, B.; Li, J. *Scripta Mater.* **1997**, *37*, 651.

(82) Huntz, A.; Huntz *J. Mater. Sci. Lett.* **1994**, *13*, 821.

(83) Cox, M. G. C.; McEnaney, B.; Scott, V. D. *Phil. Mag.* **1972**, *26*, 839.

(84) Wild, R. K. *Corros. Sci.* **1977**, *17*, 87.

(85) Quadakkers, W. J.; Piron-Abellan, J.; Shemet, V.; Singheiser, L. *Mater. High Temp.* **2003**, *20*, 115.

(86) Fergus, J. W. *Mater. Sci. Eng., A* **2005**, *397*, 271.

(87) Sabioni, A. C. S.; Huntz, A. M.; Borges, L. C.; Jomard, F. *Philos. Mag.* **2007**, *87*, 1921.

(88) Gilewicz-Wolter, J.; Dudała, J.; Żurek, Z.; Homa, M.; Lis, J.; Wolter, M. *J. Phase Equilib. Diff.* **2005**, *26*, 561.

(89) Horita, T.; Yamaji, K.; Xiong, Y.; Kishimoto, H.; Sakai, N.; Yokokawa, H. *Solid State Ionics* **2004**, *175*, 157.

(90) Horita, T.; Kishimoto, H.; Yamaji, K.; Xiong, Y.; Brito, M. E.; Yokokawa, H.; Baba, Y.; Ogasawara, K.; Kameda, H.; Matsuzaki, Y.; Yamashita, S.; Yasuda, N.; Uehara, T. *Solid State Ionics* **2008**, *179*, 2216.

(91) Schramm, B. C.; Scheerer, H.; Hoche, H.; Broszeit, E.; Abele, E.; Berger, C. *Surf. Coat. Technol.* **2004**, *188-189*, 623.

(92) Paternoster, C.; Fabrizi, A.; Cecchini, R.; El Mehtedi, M.; Choquet, P. *J. Mater. Sci.* **2008**, *43*, 3377.

(93) Issartel, C.; Buscail, H.; Caudron, E.; Cueff, R.; Riffard, F.; Perrier, S.; Jacquet, P.; Lambertin, M. *Corros. Sci.* **2004**, *46*, 2191.

(94) Issartel, C.; Buscail, H.; Caudron, E.; Cueff, R.; Riffard, F.; El Messki, S.; Perrier, S.; Jacquet, P.; Lambertin, M. *Appl. Surf. Sci.* **2004**, *225*, 14.

(95) Brady, M. P.; Weisbrod, K.; Paulauskas, I.; Buchanan, R. A.; More, K. L.; Wang, H.; Wilson, M.; Garzon, F.; Walker, L. R. *Scripta Mater.* **2004**, *50*, 1017.

(96) Brady, M. P.; Wang, H.; Yang, B.; Turner, J. A.; Bordignon, M.; Molins, R.; Abd Elhamid, M.; Lipp, L.; Walker, L. R. *Int. J. Hydrogen Energ.* **2007**, *32*, 3778.

(97) Yang, B.; Brady, M. P.; Wang, H.; Turner, J. A.; More, K. L.; Young, D. J.; Tortorelli, P. F.; Payzant, E. A.; Walker, L. R. *J. Power Sources* **2007**, *174*, 228.

(98) Nam, D.-G.; Lee, H.-C. *J. Power Sources* **2007**, *170*, 268.

(99) Gannon, P. E.; Tripp, C. T.; Knospe, A. K.; Ramana, C. V.; Deibert, M.; Smith, R. J.; Gorokhovsky, V. I.; Shutthanandan, V.; Gelles, D. *Surf. Coat. Tech.* **2004**, *188-189*, 55.

(100) Han, S.; Young, D. J. *Oxid. Met.* **2001**, *55*, 223.

(101) Young, D. J. *Mater. Sci. Forum* **2011**, *696*, 1.

(102) Armstrong, T. R.; Hardy, J. S.; Simner, S. P.; Stevenson, J. W. *Proc. - Electrochem. Soc.* **1999**, *99-19*, 706.

(103) Fergus, J. W. *Solid State Ionics* **2004**, *171*, 1.

(104) Kofstad, P.; Bredesen, R. *Solid State Ionics* **1992**, *52*.

(105) Kadowaki, T.; Shiomitsu, T.; Matsuda, E.; Nakagawa, H.; Tsuneizumi, H.; Maruyama, T. *Solid State Ionics* **1993**, *67*, 65.

(106) Kofstad, P. *Mater. Sci. Forum* **1994**, *154*, 99.

(107) Quadakkers, W. J.; Greiner, H.; Köck, W. In *1st European Solid Oxide Fuel Cell Forum* 1994; Vol. 1.

(108) Winkler, W.; Koeppen, J. *J. Power Sources* **1996**, *61*, 201.

(109) England, D. M.; Virkar, A. V. *J. Electrochem. Soc.* **1999**, *146*, 3196.

(110) Jian, L.; Jian, P.; Bing, H.; Xie, G. *J. Power Sources* **2006**, *159*, 641.

(111) Geng, S. J.; Zhu, J. H.; Lu, Z. G. *Solid State Ionics* **2006**, *177*, 559.

(112) Geng, S.; Zhu, J. *J. Power Sources* **2006**, *160*, 1009.

(113) Ivers-Tiffee, E.; Wersing, W.; Schiessl, M.; Greiner, H. *Ber. Bunsen-Ges. Phys. Chem.* **1990**, *94*, 978.

(114) Huczkowski, P.; Shemet, V.; Piron-Abellan, J.; Singheiser, L.; Quadakkers, W. J.; Christiansen, N. *Mater. Corros.* **2004**, *55*, 825.

(115) Linderoth, S.; Larsen, P. H. *Mater. Res. Soc. Symp. Proc.* **2000**, *575*, 325.

(116) Malkow, T.; Crone, U. V. D.; Laptev, A. M.; Koppitz, T.; Breuer, U.; Quadakkers, W. J. *Proc. - Electrochem. Soc.* **1997**, *97-40*, 1244.

(117) Zhu, W.-z.; Yan, M. *J. Zhejiang Univ., Sci.* **2004**, *5*, 1471.

(118) Asteman, H.; Segerdahl, K.; Svensson, J.-E.; Johansson, L.-G. *Mater. Sci. Forum* **2001**, *5*, 369.

(119) Hilpert, K.; Das, D.; Miller, M.; Peck, D. H.; Weiss, R. *J. Electrochem. Soc.* **1996**, *143*, 3642.

(120) Quadakkers, W. J.; Greiner, H.; Haensel, M.; Pattanaik, A.; Khanna, A. S.; Mallener, W. *Solid State Ionics* **1996**, *91*, 55.

(121) Yokokawa, H.; Horita, T.; Sakai, N.; Yamaji, K.; Brito, M. E.; Xiong, Y. P.; Kishimoto, H. *Solid State Ionics* **2006**, *177*, 3193.

(122) Fergus, J. W. *Int. J. Hydrogen Energ.* **2007**, *32*, 3664.

(123) Meulenberg, W. A.; Uhlenbruck, S.; Wessel, E.; Buchkremer, H. P.; Stoever, D. *J. Mater. Sci.* **2003**, *38*, 507.

(124) Crofer 22 APU, Material Data Sheet No.4046, ThyssenKrupp VDM, **2005.**

(125) Antepara, I.; Villarreal, I.; Rodríguez-Martínez, L. M.; Lecanda, N.; Castro, U.; Laresgoiti, A. *J. Power Sources* **2005**, *151*, 103.

(126) Chiu, Y.-T.; Lin, C.-K. *Journal of Power Sources* **2012**, *198*, 149.

(127) Palcut, M.; Mikkelsen, L.; Neufeld, K.; Chen, M.; Knibbe, R.; Hendriksen, P. V. *Corros. Sci.* **2010**, *52*, 3309.

(128) Crofer 22 APU, Material Data Sheet No.4046, **2005.**

(129) Sanergy HT, Material Data Sheet, Sandvik Materials Technology, **2007**

(130) Fergus, J. W.; Zhao, Y.; Haney, R.; Cramer, K.; Riherd, L. *ECS Trans.* **2010**, *25*, 101.

(131) Yang, Z.; Xia, G.-G.; Wang, C.-M.; Nie, Z.; Templeton, J.; Stevenson, J. W.; Singh, P. *J. Power Sources* **2008**, *183*, 660.

(132) Chung, J. H.; Huh, J. Y.; Jun, J. H.; Kim, D. H.; Jun, J.-H. *Adv. Mater. Res. (Zuerich, Switz.)* **2007**, *15-17*, 305.

(133) Garcia-Vargas, M. J.; Lelait, L.; Kolarik, V.; Fietzek, H.; Juez-Lorenzo, M. d. M. *Mater. High Temp.* **2005**, *22*, 245.

(134) Fontana, S.; Chevalier, S.; Caboche, G. *J. Power Sources* **2009**, *193*, 136.

(135) Larring, Y.; Haugsrud, R.; Norby, T. *J. Electrochem. Soc.* **2003**, *150*, B374.

(136) Quadakkers, W. J.; Piron-Abellan, J.; Shemet, V.; Singheiser, L. *Mater. High Temp.* **2003**, *20*, 115.

(137) Sakai, N.; Horita, T.; Xiong, Y. P.; Yamaji, K.; Kishimoto, H.; Brito, M. E.; Yokokawa, H.; Maruyama, T. *Solid State Ionics* **2005**, *176*, 681.

(138) Kofstad, P.; Risoe National Laboratory: **1996**, 55.

(139) Brylewski, T.; Maruyama, T.; Nanko, M.; Przybylski, K. *J. Therm. Anal. Calorim.* **1999**, *55*, 681.

(140) Piccardo, P.; Chevalier, S.; Molins, R.; Viviani, M.; Caboche, G.; Barbucci, A.; Sennour, M.; Amendola, R. *Surf. Coat. Technol.* **2006**, *201*, 4471.

(141) Liu, Y. *J. Power Sources* **2008**, *179*, 286.

(142) Yen, S. K.; Tsai, Y. C. *J. Electrochem. Soc.* **1996**, *143*, 2736.

(143) Nakagawa, K.; Matsunaga, Y.; Yanagisawa, T. *Mater. High Temp.* **2003**, *20*, 67.

(144) Kurokawa, H.; Oyama, Y.; Kawamura, K.; Maruyama, T. *Proc. - Electrochem. Soc.* **2003**, *2003-16*, 170.

(145) Yang, Z.; Xia, G.; Singh, P.; Stevenson, J. W. *Solid State Ionics* **2005**, *176*, 1495.

(146) Yang, Z.; Xia, G.-G.; Walker, M. S.; Wang, C.-M.; Stevenson, J. W.; Singh, P. *Int. J. Hydrogen Energ.* **2007**, *32*, 3770.

(147) Holcomb, G.; Ziomek-Moroz, M.; Cramer, S.; Covino, B.; Bullard, S. *J. Mater. Eng. Perform.* **2006**, *15*, 404.

(148) Huang, W.; Gopalan, S.; Pal, U. B.; Basu, S. N. *ECS Trans.* **2007**, *7*, 2379.

(149) Norby, T. *Adv. Ceram.* **1987**, *23*, 107.

(150) Kofstad, P. *Oxid. Met.* **1995**, *44*, 3.

(151) Hultquist, G.; Tveten, B.; Hörnlund, E. *Oxid. Met.* **2000**, *54*, 1.

(152) Gannon, P. E.; White, P. T. *ECS Trans.* **2009**, *16*, 53.

(153) Essuman, E; Meier, G. H.; Zurek, J.; Hänsel, M.; Singheiser, L.; Quadakkers, W. J. *Scripta. Mater.* **2007**, *57*, 845

(154) Ehlers, J.; Young, D. J.; Smaardijk, E. J.; Tyagi, A. K.; Penkalla, H. J.; Singheiser, L.; Quadakkers, W. J. *Corros. Sci.* **2006**, *48*, 3428.

(155) Fu, C. J.; Sun, K. N.; Zhang, N. Q.; Chen, X. B.; Zhou, D. R. *Thin Solid Films* **2008**, *516*, 1857.

(156) Yang, Z.; Xia, G.-G.; Maupin, G. D.; Stevenson, J. W. *Surf. Coat. Technol.* **2006**, *201*, 4476.

(157) Fontana, S.; Amendola, R.; Chevalier, S.; Piccardo, P.; Caboche, G.; Viviani, M.; Molins, R.; Sennour, M. *J. Power Sources* **2007**, *171*, 652.

(158) Chu, C.-L.; Wang, J.-Y.; Lee, S. *International Journal of Hydrogen Energy* **2008**, *33*, 2536.

(159) Shaigan, N.; Ivey, D. G.; Chen, W. *J. Power Sources* **2008**, *185*, 331.

(160) Yang, Z.; Xia, G.; Simner, S. P.; Stevenson, J. W. *J. Electrochem. Soc.* **2005**, *152*.

(161) Montero, X.; Tietz, F.; Sebold, D.; Buchkremer, H. P.; Ringuede, A.; Cassir, M.; Laresgoiti, A.; Villarreal, I. *J. Power Sources* **2008**, *184*, 172.

(162) Alvarez, E.; Meier, A.; Weil, K. S.; Yang, Z. *Int. J. Appl. Ceram. Technol.* **2010**, *8*, 33.

(163) Hua, B.; Kong, Y. H.; Lu, F. S.; Zhang, J. F.; Pu, J.; Li, J. *Chin. Sci. Bull.* **2010**, *55*, 3831.

(164) Yang, Z.; Xia, G.-G.; Li, X.-H.; Stevenson, J. W. *Int. J. Hydrogen Energ.* **2007**, *32*, 3648.

(165) Xin, X.; Wang, S.; Zhu, Q.; Xu, Y.; Wen, T. *Electrochem. Commun.* **2010**, *12*, 40.

(166) Balland, A.; Gannon, P.; Deibert, M.; Chevalier, S.; Caboche, G.; Fontana, S. *Surf. Coat. Technol.* **2009**, *203*, 3291.

(167) Uehara, T.; Yasuda, N.; Okamoto, M.; Baba, Y. *J. Power Sources* **2011**, *196*, 7251.

(168) Stanislowski, M.; Froitzheim, J.; Niewolak, L.; Quadakkers, W. J.; Hilpert, K.; Markus, T.; Singheiser, L. *J. Power Sources* **2007**, *164*.

(169) Shaigan, N.; Qu, W.; Ivey, D. G.; Chen, W. *J. Power Sources*, *195*, 1529.

(170) Froitzheim, J.; Svensson, J. E. *Mater. Sci. Forum* **2011**, *696*, 412.

(171) Froitzheim, J.; Svensson, J. E. *ECS Trans.* **2011**, *35*, 2503.

(172) Yen, S. K.; Taai, Y. C. *J. Electrochem. Soc.* **1996**, *143*, 2736.

(173) Zurek, J.; Meier, G. H.; Essuman, E.; Hänsel, M.; Singheiser, L.; Quadakkers, W. J. *J. Alloys Compd.* **2009, 467, 450.**

(174) Quadakkers, W. J.; Huczkowski, P.; Naumenko, D.; Zurek, J.; Meier, G. H.; Niewolak, L.; Singheiser, L. *Mater. Sci. Forum* **2008**, 595-598, 1111.